GEOFISICA INTERNACIONAL

REVISTA DE LA UNION GEOFISICA MEXICANA, AUSPICIADA POR EL INSTITUTO DE GEOFISICA DE LA UNIVERSIDAD NACIONAL AUTONOMA DE MEXICO

Vol. 19 México, D.F., 1o. de julio de 1980 Núm. 3

AN INTERCOMPARISON OF THE THERMAL EMISSION FIELDS FOR THE PLANETS

K. YA. KONDRATYEV*
N. I. MOSCALENKO*

(Received June 25, 1980)

RESUMEN

Se presenta una comparación de los campos de emisión térmica de la Tierra, Marte, Venus y Júpiter. Los métodos de cálculo utilizados toman en cuenta la composición química real de la atmósfera y las condiciones atmosféricas para los diferentes planetas estudiados. Los campos de emisión térmica se obtienen para atmósferas clara, turbia y nubosa. Los cálculos incorporan esfericidad, refracción atmosférica, selectividad de la radiación incidente reflejada por la superficie y las nubes, así como selectividad de la radiación dispersada por aerosol para resolución espectral baja y moderada, considerando el efecto de todos los componentes gaseosos sobre la transferencia de radiación.

Los resultados obtenidos y las conclusiones derivadas revelan regularidades generales y rasgos específicos de la formación de la emisión térmica de los planetas.

* *Voeikov Main Geophysical Observatory, Leningrad, URSS.*

ABSTRACT

A comparison of the thermal emission fields of the Earth, Mars, Venus and Jupiter is presented. The calculation methods used take into account the real chemical composition of the atmosphere and the atmospheric conditions for the different planets studied. Thermal emission fields are obtained for clear, turbid and cloudy atmospheres. The calculations take into account sphericity, atmospheric refraction, selectivity of the downward radiation reflected by the underlying surface and clouds and selectivity of radiation scattered by aerosol for low and moderate resolutions, considering the effect of all gaseous components on radiation transfer.

The results obtained and the conclusions drawn reveal the general regularities and specific features of the formation of the planets' thermal emission.

During the last decade the planets of the solar system have been intensively studied with the help of the ground-based astronomic instruments, satellites and interplanetary automatic stations. Various techniques of direct measurements and remote sounding have made it possible to obtain information on the chemical composition and vertical structure of the atmospheres of Earth, Venus, Mars and Jupiter. This information has been discussed in the monographs and reviews by Kondratyev (1976, 1977), Kondratyev and Moscalenko (1974, 1977), Kuzmin and Marov (1974), Moroz (1978) and others. Accumulation of observational data on atmospheric and surface conditions on planets (first of all on the chemical composition and vertical temperature profiles for different climatic zones and seasons) and successful solution by Moscalenko *et al.* (1969, 1970, 1978, 1979) of the problem of the spectral transmission functions for the atmospheres have made it possible to theoretically analyze the fields of the down and upward atmospheric thermal emission, to determine the basic features of their spectral and spatial structure, to reveal the extent of the influence of various meteorological factors on the spatial-temporal variability of the emission fields. An important contribution to these studies was made by Kondratyev and Bunakova (1973), Kondratyev and Moscalenko (1974, 1975, 1976), Kondratyev, Moscalenko and Yakupova (1979), Moscalenko (1975, 1976), and Moscalenko and Zakirova (1972, 1975).

The present paper compares the fields of the planets' thermal emission to reveal general regularities and specific features of their formation. The results obtained and the conclusions drawn are based on the detailed analysis of the computed data on the spectral and spatial structures of the thermal emission fields for Earth, Mars, Venus, and Jupiter.

The Techniques for Approximate Calculation of the Thermal Emission Fields

To correctly take into account a real chemical composition of the atmospheres and atmospheric conditions for different planets, several techniques were developed to calculate the thermal emission fields for clear, turbid and cloudy atmospheres. Calculation techniques were developed with due regard to sphericity and refraction in an atmosphere, selectivity of the downward radiation reflected by the underlying surface and clouds, selectivity of radiation scattered by aerosol, for low, $\Delta = 30 - 100$ cm $^{-1}$, and moderate, $\Delta = 2 - 5$ cm^{-1}, resolutions, considering the effect of all gaseous components on radiation transfer. In particular, in the case of terrestrial atmosphere, one took into account radiation absorption by water vapour (Continuum absorption included), CO_2, O_3, N_2O, CO, CH_4, NO, NO_2, NH_3, HNO_3, SO_2, C_2H_2, and induced absorption by colliding molecules $N_2 - N_2$ and $N_2 - O_2$.

Spectral transmission functions in the calculation techniques were computed with the use of one-parameter and two-parameter techniques of equivalent absorbing mass. The transmission function parameters were determined from the results of complex measurements made with mean and high resolutions for wide ranges of temperatures, pressures and abundances of radiation-absorbing gaseous components. For absorption bands of water vapour, CO_2, N_2O, O_3, CO, CH_4, NO with spectral resolution $\Delta \leqslant 3$ cm^{-1} the data were used on transmission functions directly (line by line) calculated by Moscalenko and Yakupova (1978). Most complicated are the calculation techniques for the thermal emission fields in conditions of a turbid atmosphere, when it is necessary to take into account spatial re-distribution of radiation due to radiation scattered in an absorbing atmosphere.

The calculation techniques for the thermal emission fields use the input information on model atmospheres in a numerical form, which enables one to calculate spectral radiances of the thermal emissions for arbitrary vertical temperature profiles, relative humidity, aerosol optical density and scattering indicatrix of aerosol, pressure and concentration of gaseous components. The height of the underlying surface and the spectral characteristic of surface albedo may be also arbitrary.

Kondratyev and Moscalenko (1976, 1977) compared the calculated and measured spectral radiances in controlled atmospheric conditions of Earth and Mars with a low spectral resolution. Additional information on the spectral radiances of the outgoing emission for Venus and Jupiter observed from aircraft and spacecraft, also testifies to a reasonable agreement with theoretical calculations.

One can also mention the results of comparison of the radiance spectra for the outgoing thermal emission in nadir calculated and observed from Nimbus 4 with

a resolution of $\Delta \approx 2$ cm^{-1} near the 15 μm CO_2 band. Complete agreement is observed between the spectral structure of the outgoing emission with a distinct maximum of emission near the Q-branch of the 15 μm CO_2 band, and a reasonable agreement between the absolute values of emission radiances. As a rule, the difference in the values of observed and calculated emissions does not exceed 10 % , provided the effect of temperature on the spectral transmission function for water vapour and continuum absorption of radiation by water vapour are taken into account.

Spatial-Temporal Variability and Spectral Structure of the Thermal Emission Field for Earth

The main features of the spectral and spatial structures of the thermal emission fields and the extent of the influence of various meteorological factors on their spatial-temporal variability can be revealed by analyzing the results of emission fields' calculations obtained for the given states of the atmosphere and surface. The latter are modelled by using the statistic information on the meteorological condition of the atmosphere for different climatic zones and seasons on Earth: 1 - ARDC model; 2 - model of moderate summer in mid-latitudes T(z=0) = 293K; 3 - model of moderate winter in mid-latitudes T(z=0) = 257.1K; 4 - model of moist tropics, T(z=0) = 299.6K; 5 - model of the tropics with a humid troposphere and a dry stratosphere, T(z=0) = 299K; 6 - model of moderate summer in mid-latitudes with a dry atmosphere, T(z=0) = 293K; 7 - model of a dry atmosphere, T(z=0) = 301.1K; 8 - model of cold winter, T(z=0) = 233K; 9 - model of moderate winter in mid-latitudes with a dry stratosphere, T(z=0) = 257.1K; 10 - model of cold summer, relative humidity of the troposphere is below average, T(z=0) = 283K; 11 - model of hot summer with varying humidity in the troposphere, T(z=0) = 301.1K; 12 - model of a desert, hot summer, noon, T(z=0) = 325K; 13 - model of a cold atmosphere in the sub-Arctic, T(z=0) = 205K.

Calculations were performed for a spectral resolution $\Delta\lambda = 0.025$; 0.05; 0.1 and 0.5 μm in the corresponding spectral intervals 2-3, 3-6, 6-18, 18-50 μm. Spectral radiances were calculated for a resolution $\Delta\nu \leqslant 2$-5 cm^{-1} only for control states of the atmosphere, selected altitudes and viewing directions.

Vertical aerosol optical thickness profiles were selected by generalizing the latest data of the ground-based, aircraft and balloon measurements of the atmospheric aerosol, including the data of laser sounding. The optical characteristics were calculated from size distribution and chemical composition of actual aerosols with due regard to its multi-component composition.

A Free Clear Atmosphere.

The spectral structure and spatial variability of the spectral radiance in these conditions are determined by the vertical temperature profile and chemical composition of the atmosphere. When the temperature of the Earth's surface is $t_s > 0^oC$, the troposphere is characterized by a negative temperature lapse rate, and the spectral radiance of the upward radiation, $\mathcal{J}_\lambda^\uparrow$ decreases with height. In the intervals corresponding to most strong absorption bands 4.3; 15μm CO_2; 6.3 μm water vapour; 4.75 and 9.6 μm O_3; 4.5 μm N_2O, radiance changes are more significant. Maxima in the $\mathcal{J}_\lambda^\uparrow$ values for the troposphere correspond to atmospheric transparency windows. The spectral structures of the upward thermal emission field for conditions with $t_s > 0$ are similar for different models, though the spectral structure of the upward emission is more clearly pronounced when the surface temperature becomes higher. When the zenith angle grows, the spectral radiances of the tropospheric upward emission decrease.

If for the atmospheric transparency windows the spectral radiances $\mathcal{J}_\lambda^\uparrow$ decrease with altitude, the strong absorption bands at altitudes $z > 30$ km may be characterized by an increase in $\mathcal{J}_\lambda^\uparrow$ with increasing altitude and growing zenith angle (Fig. 2) due to a contribution of the emission in warmer stratospheric layers in the region of temperature inversion at altitudes exceeding 30 km.

The increasing of the spectral resolution (Fig. 1) does not change the general character of spectral and spatial structures of the upward thermal emission. But their details determined by minor absorbing atmospheric components in spectral regions with most strong absorption, are more clearly pronounced. So, for instance, most clearly seen are Q-branches of the 10 μm NH_3 band; 7.8 and 8.6 μm N_2O and 7.6 μm CH_4 bands. A higher spectral resolution enables one to select the intervals free of water vapour absorption and to use them to estimate the content of minor components from the values of spectral radiances of the outgoing thermal emission at a resolution of $\Delta \leqslant 0.5 - 1$ cm^{-1}. At such resolution, details of the spectral structure are pronounced in the upward emission radiances, which are determined, for instance, by sulphuric gas, acetylene, HNO_3 vapour, freons, etc.

In conditions of the cold atmosphere of the Arctic and Antarctic, the spectra of the upward thermal emission in the spectral intervals with a strong atmospheric absorption have an emissive character (Fig. 3) due to the near-ground atmospheric inversion and emission of warmer stratospheric layers. As the zenith angle grows, the spectral intervals of the atmospheric emission broaden.

In the general case, the spectral distribution of $\mathcal{J}_\lambda^\uparrow$ depends considerably on the

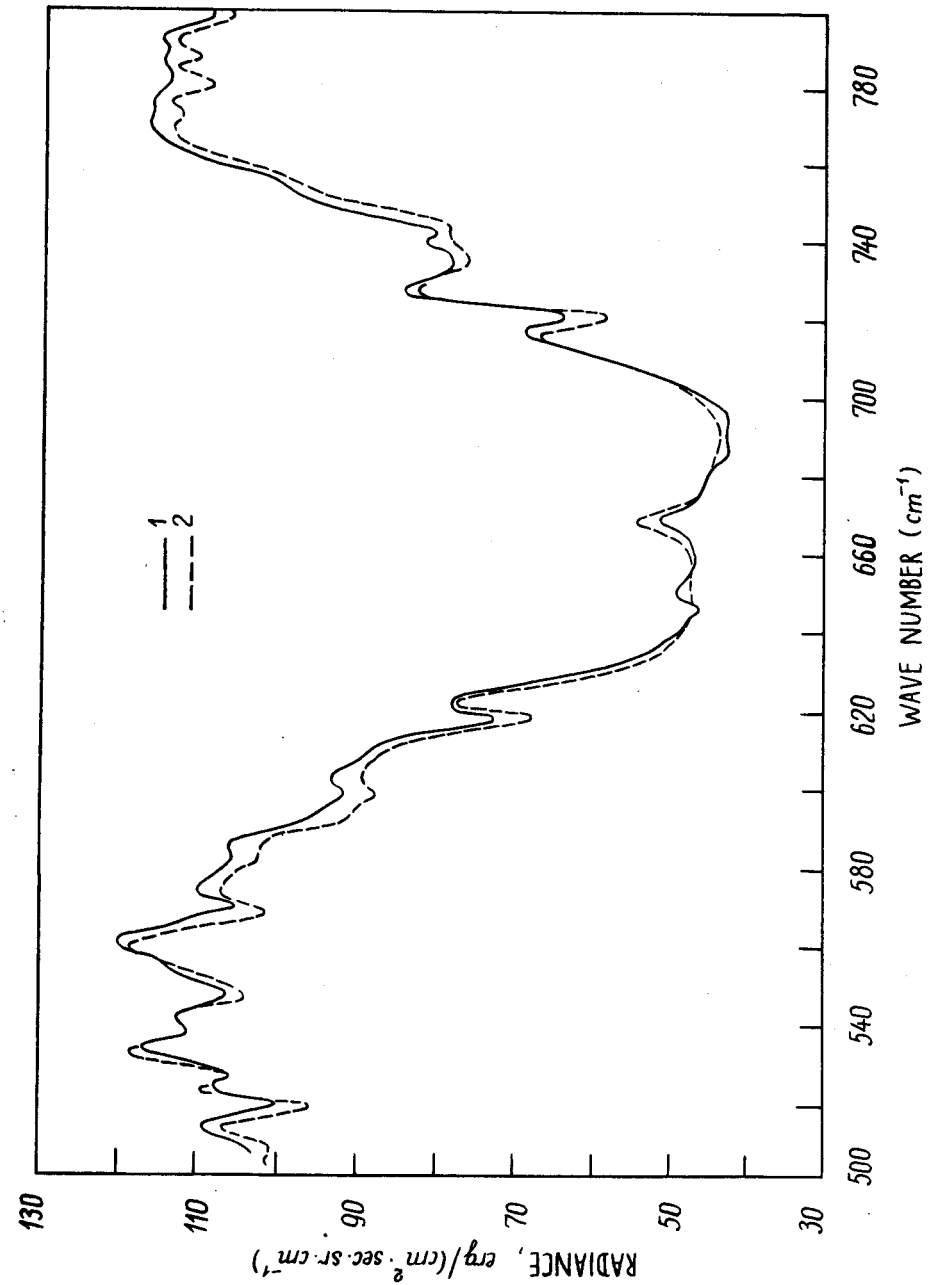

Fig. 1 Comparison of the observed (1) and calculated (2) radiance spectra for the outgoing emission of the Earth in nadir direction.

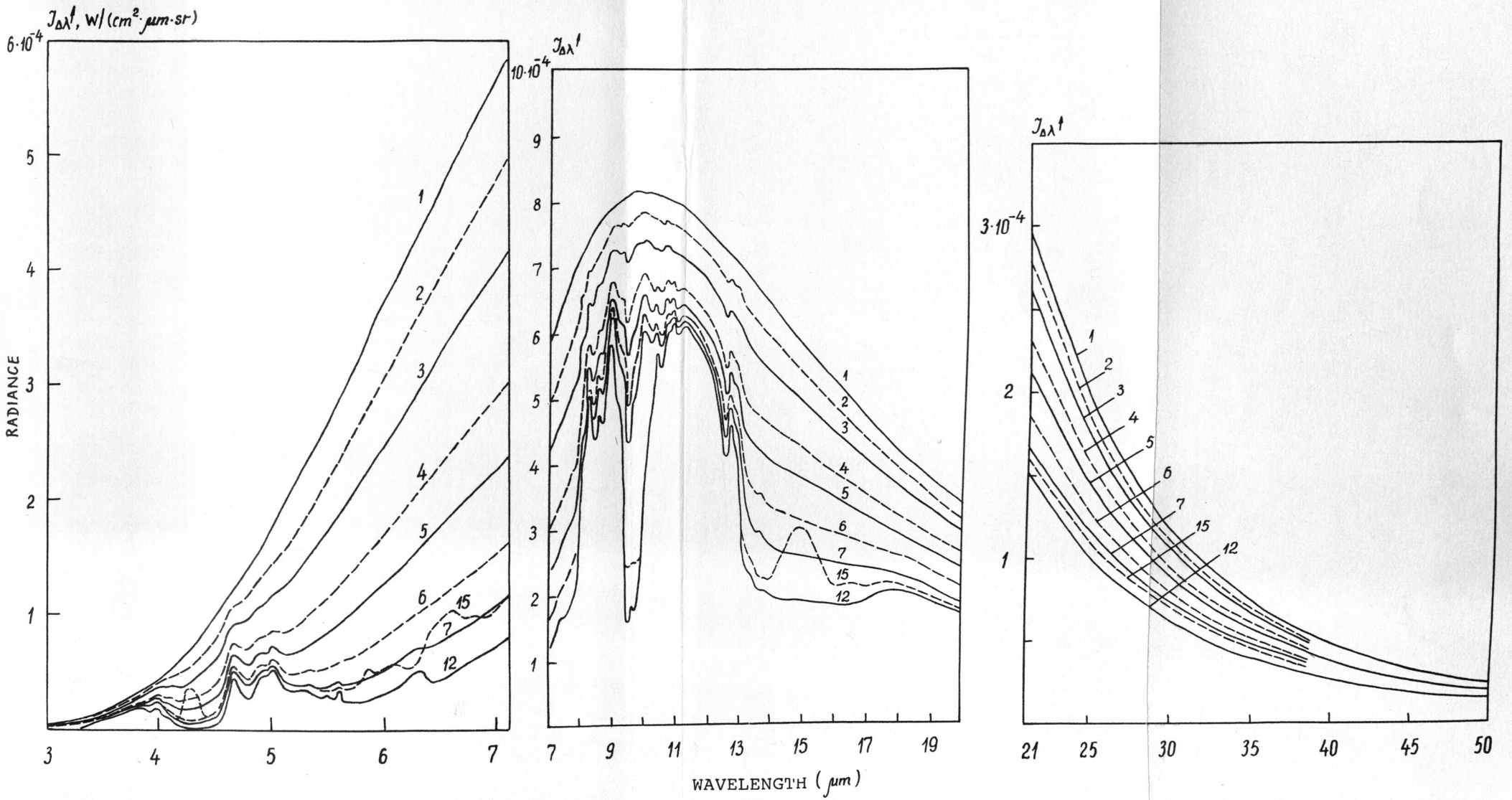

Fig. 2 Spectral radiance of the upward thermal emission of Earth $J_\lambda\uparrow$ at different altitudes in a cloud-free clear atmosphere, model 1, $\theta = 85^\circ$.
Height, z, km: 1-0.1; 2-1; 3-2; 4-3.7; 5-5; 6-6.8; 7-8.6; 8-20.4; 9-52.
a) spectral region 3 - 7 μm;
b) 7 - 20 μm; c) 21 - 25 μm.

zenith angle and atmospheric stratification. In conditions of the terrestrial atmosphere, a tendency is observed to decreasing radiance of the upward emission as the temperatures of the near-ground atmosphere and the surface become lower. Temperature contrasts between various model atmospheres play a decisive role in variability of the upward emission.

Spectral radiance of the downward atmospheric emission, $\mathcal{I}_\lambda^{\downarrow}$ (Fig. 4) depends to a greater extent on the zenith angle and reflects spectral variations of atmospheric absorptivity. One can trace in the emission spectra not only the bands but also the details of their spectral structure. So, for instance, one can easily trace the bands of water vapour (2.7; 3.2 and 6.3 μm), CO_2 (2; 2.7; 4.3; 9.4; 10.4; 15 μm), N_2O (4.5; 7.8 μm), CH_4 (3.3; 7.6 μm), and O_3 (4.75; 9.6 μm). In the absence of temperature anomalies in the atmosphere, the spectral radiance of $\mathcal{I}_\lambda^{\downarrow}$ decreases with height and increases with growing zenith angle in the band wings, while in the spectral intervals with strong absorption the value of $\mathcal{I}_\lambda^{\downarrow}(\theta)$ remains almost constant. As the height increases, the spectral ranges, in which the zenith angle-dependence of $\mathcal{I}_\lambda^{\downarrow}$ shows itself, broaden. At $z > 10$ km, the $\mathcal{I}_\lambda^{\downarrow}(\theta)$ dependences are pronounced in all the spectral intervals, except near the 4.26 μm wavelength, corresponding to the most strong CO_2 absorption band. Relative humidity and distribution of gaseous components affect to a greater extent the spectral structure and angular dependence of $\mathcal{I}_\lambda^{\downarrow}$ as compared to $\mathcal{I}_\lambda^{\uparrow}$. In the spectral intervals with strong atmospheric absorption, variations of radiances with height correlate with temperature contrasts in the atmosphere.

The Turbid Atmosphere

An atmospheric aerosol affects the formation of the thermal emission field through the mechanism of emission (in the bands of radiation absorption by aerosol) and the mechanism of scattering. The role of all the types of aerosol in the mechanism of thermal emission generation depends significantly on absorptivity of atmospheric gaseous components. In the spectral intervals with strong atmospheric absorption, the aerosol weakly affects the spectral structure and spatial distribution of the upward and downward emission. In atmospheric transparency windows (the spectral intervals 3-4.1; 4.6-5.2; 7.6-13.5 μm) the effect of aerosol on spectral radiances of $\mathcal{I}_\lambda^{\downarrow\uparrow}$ shows itself stronger.

As Kondratyev and Moscalenko (1977) showed, the spectral radiances of the upward emission, $\mathcal{I}_\lambda^{\uparrow}$, in atmospheric windows depend weaker on the zenith angle as compared to the downward emission. Therefore, scattering properties of the aerosol are weaker pronounced in $\mathcal{I}_\lambda^{\uparrow}$ (in the spectral regions where $\mathcal{I}_\lambda(\theta) =$ const, the effect of aerosol scattering properties should not be pronounced at all). The aerosol's ability to absorb the i.r. radiation has a decisive effect on $\mathcal{I}_\lambda^{\uparrow}$, and

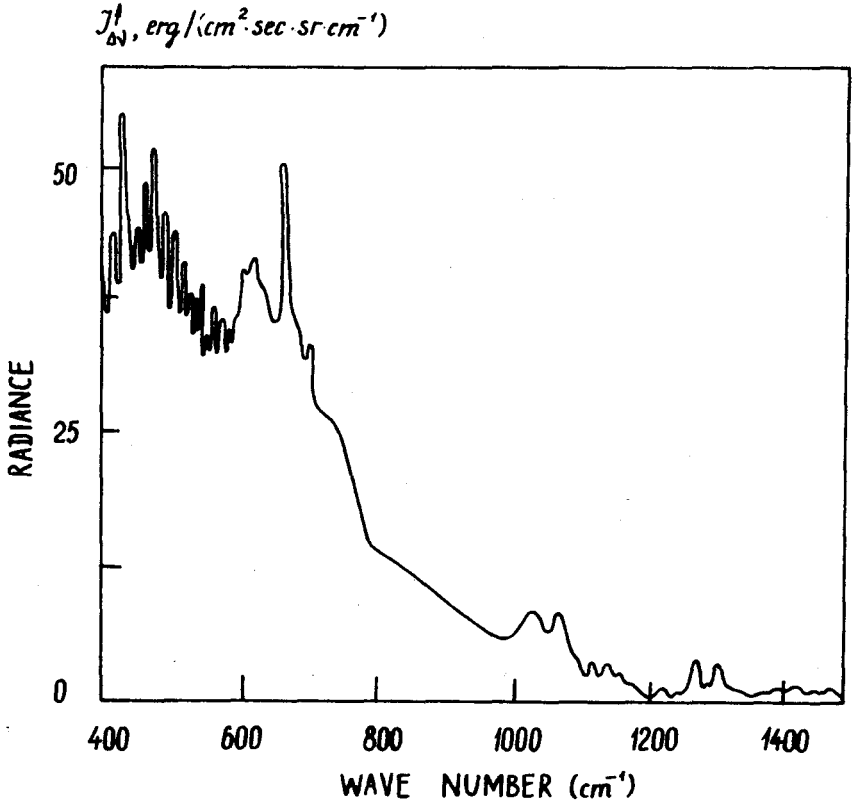

Fig. 3 Spectral radiance of the outgoing thermal emission of the Earth for atmospheric model 13 and nadir viewing.

the aerosol with clearly pronounced absorption bands may considerably affect the spectral structure of $J_\lambda^{\uparrow}$. The absorption bands are more clearly pronounced in the case of fine-dispersive (submicrone) aerosol, which, as Moscalenko and Terzi (1979) show, affects the transformation of the $J_\lambda^{\downarrow\uparrow}$ thermal emission radiances only through the absorption mechanism. Since the aerosol spectral absorption function A_λ grows faster with increasing zenith angle as compared to the growth of A_λ for absorption by atmospheric gases, the effect of aerosol on $J_\lambda^{\uparrow}$ increases with increasing zenith angle. In mid-latitudes with a moderate and high humidity, aerosol in the surface layer consists mainly of particles of water and water solutions affecting the radiances of the upward emission in the spectral regions 3.0-3.5 and 8.5-13.5 μm. Higher layers of the tropospheric aerosol (0.5-3 km) involve particles of water solutions, mineral aerosol and particles of amonia sulfate. This layer leads to a more significant decrease of the upward emission in the 7.8-13.59 μm spectral

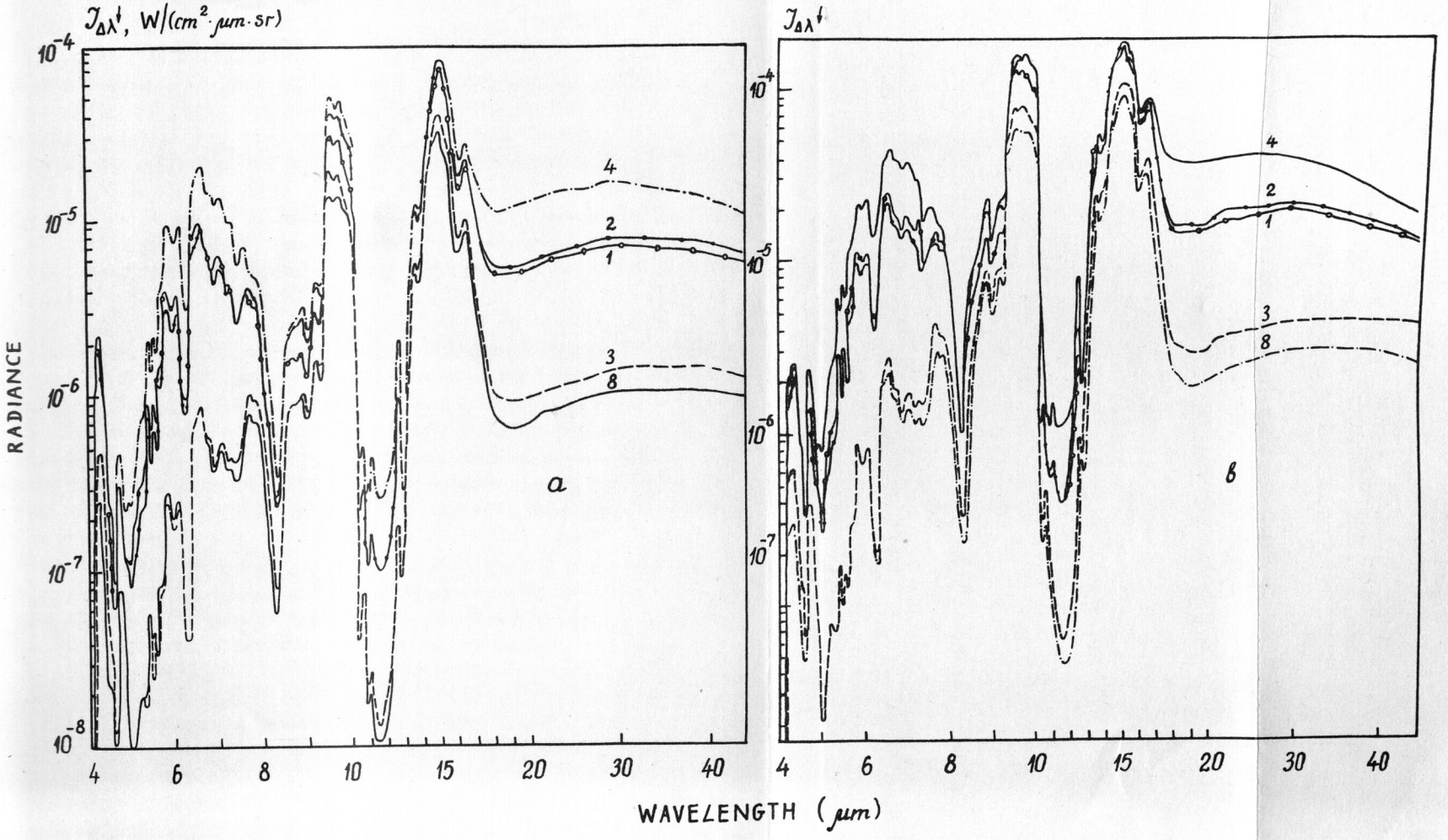

Fig. 4 Spectral radiance of the downward emission in the Earth's atmosphere in the 4-45 μm spectral region for atmospheric stratifications 1-4 and 8 at the altitude z = 25 km;
a) $\theta = 0^{o}$; b) $\theta =$
a) $\theta = 0^{o}$; b) $\theta = 85^{o}$.

region. In the case of a very turbid lower troposphere, the effect of the background tropospheric aerosol and stratospheric aerosol in mid-latitudes shows itself weakly in $\mathcal{J}_\lambda^\uparrow(z, \theta)$ dependences.

The aerosol in a layer with an active turbulent exchange (0-2km) over the sea is more large-dispersive (large-size) as compared to the continental aerosol, and in atmospheric transparency windows it attenuates the emission much strongerly through a mechanism of scattering*. In this connection, the marine aerosol affects weakerly the radiance of the upward and outgoing emission as compared to the continental aerosol. The effect of the marine aerosol on $\mathcal{J}_\lambda^\uparrow$ shows itself only in the 8.2-9 μm spectral region. In these conditions it is important to take account of the contribution of higher aerosol layers into radiative transfer, namely, the background tropospheric and stratospheric layers characterized by strong absorption bands in the spectral region $\lambda > 9$ μm.

The aerosol above arid and subarid regions affects most strongly the transformation of the upward and outgoing thermal emission of the Earth, especially in dust-storm conditions, when the optical thickness of an aerosol column may reach $\tau = 1.2$. The authors calculated the thermal emission fields for conditions of the dust aerosol for three vertical profiles ρ_τ (z) of the aerosol optical thickness shown in Table 1. The first vertical profile ρ_τ (I) corresponds to a weakly turbid atmosphere prior to a dust storm and to a smaller-size aerosol; ρ_τ (II) corresponds to a mature dust storm, when the dust cloud is lifted up by a powerful vertical flow being involved into a high-altitude atmospheric circulation (this case is characterized by a larger-size aerosol); ρ_τ (III) corresponds to the conditions of dust-storm subsidence, when the largest dust particles fall out of the dust cloud, and the cloud itself is being dissipated by vertical and horizontal circulation processes.

Figure 5 compares the radiances of the outgoing thermal emission for conditions of clear and turbid atmospheres according to three above-mentioned models of the atmospheric aerosol. A circumstance attracts attention that in conditions of a dust storm an increase in the aerosol optical thickness and large particles' fraction leads to qualitatively similar variations of the thermal emission spectral structure. The latter is determined by approximately proportional increase in the coefficients of scattering and absorption of the dust aerosol in the 7.6-14 μm spectral region. In the spectral regions 8.5-11 and 18-22 μm, the dust aerosol considerably affects $\mathcal{J}_\lambda^\uparrow$.

* The increase of scattering coefficients is determined by considerable abundance of NaCl and KCl salts transparent in the 8-14 μm i.r. region, in the aerosol chemical composition.

TABLE 1

Vertical Profiles of the Atmospheric Aerosol's Optical Thickness in Arid and Subarid Zones.

z, km	ρ_α			z, km	ρ_α		
	I	II	III		I	II	III
0	0.1	0.6	0.05	5.0	0.02	0.028	0.05
0.5	0.05	0.45	0.07	6.0	0.018	0.020	0.018
1.0	0.05	0.32	0.1	7.0	0.016	0.016	0.016
2.0	0.05	0.17	0.1	8.0	0.014	0.014	0.014
3.0	0.05	0.085	0.1	9.0	0.013	0.013	0.013
4.0	0.05	0.047	0.1	10.0	0.011	0.011	0.011

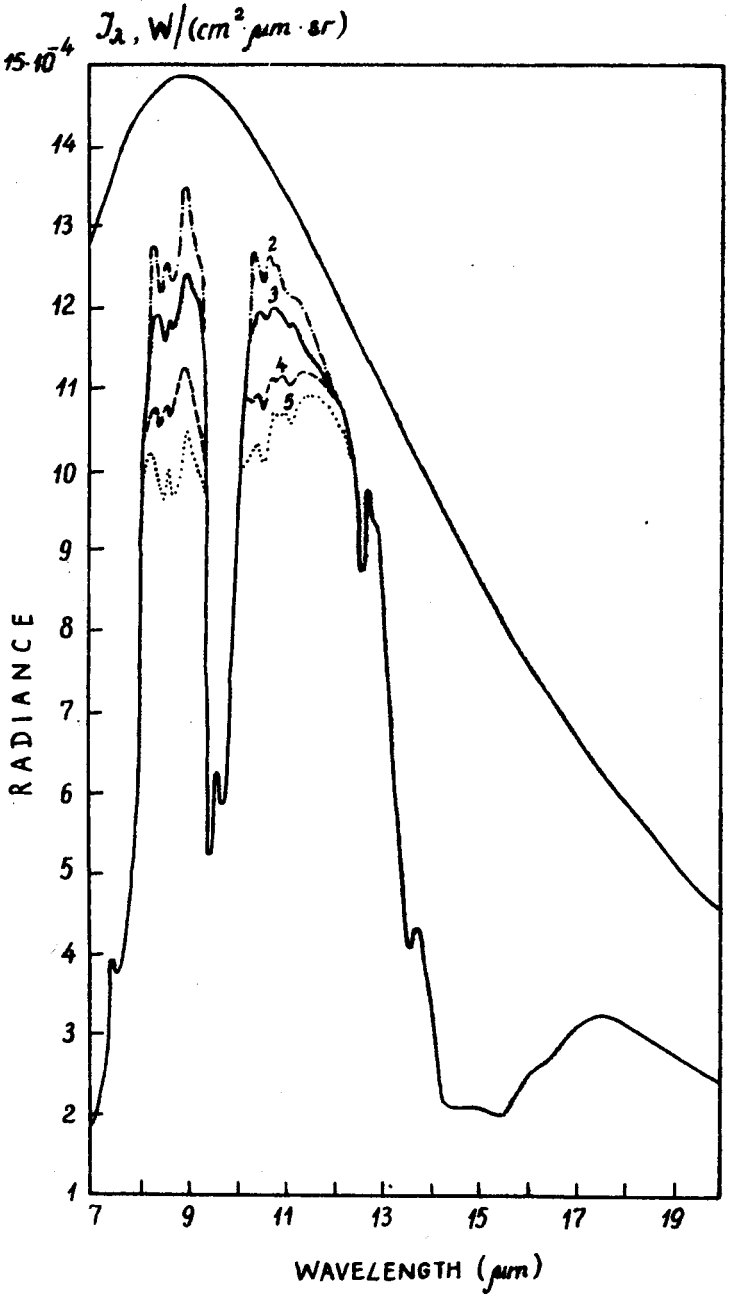

Fig. 5 Spectral radiance of the outgoing thermal emission of the Earth for nadir viewing in the 7-20 μm region for atmospheric model 12.
1 - the underlying surface emission;
2 - clear atmosphere;
3, 4, 5 - turbid atmosphere for models 1, 3, 2, respectively.

Over the West Europe and the industrial regions of the USA the aerosol in the active turbulent exchange zone is of industrial origin and strongly absorbs in the 2.6-3.5 and 7.2-25 μm spectral regions, centered at 2.9, 9 and 18 μm, near which the transformation of the thermal emission spectral radiance is most strongly pronounced.

When the atmospheric turbidity grows, the upward emission decreases at all zenith angles. The aerosol effect on the spectral structure and spatial distribution of the downward thermal emission shows itself stronger and is caused not only by the absorption mechanism, but also by the scattering mechanism. This effect greatly depends on the ratio between spectral coefficients of absorption and scattering by aerosol and on the shape of the phase function. As a rule, elongation of the phase function decreases with increasing wavelength. Therefore, the mechanism for the thermal emission scattering by aerosol with its subsequent directional redistribution should be taken into account first of all in the longwave 8-14 μm transparency window.

According to the calculational technique proposed by Moscalenko (1975), the downward emission radiance, $\mathcal{I}_\lambda^\downarrow$, is calculated using the formula

$$\mathcal{I}_\lambda^\downarrow = \mathcal{I}_{1\lambda}^\downarrow + \mathcal{I}_{2\lambda}^\downarrow + \mathcal{I}_{3\lambda}^\downarrow + \mathcal{I}_{4\lambda}^\downarrow + \mathcal{I}_{5\lambda}^\downarrow$$

where $\mathcal{I}_{1\lambda}^\downarrow(z, \theta)$ is the radiance of the downward emission in the direction $\theta(z)$ (with due regard to emissions of atmospheric gases and aerosols) attenuated by aerosol scattering; $\mathcal{I}_{2\lambda}^\downarrow(z, \theta)$ is the radiance of the downward atmospheric emission scattered in the direction $\theta(z)$ and reaching the observational point z; $\mathcal{I}_{3\lambda}^\downarrow(z, \theta)$ is the radiance of the horizon's emission scattered in the direction $\theta(z)$, reaching the observational point z ; $\mathcal{I}_{4\lambda}^\downarrow$ is the radiance of the backscattered upward emission of the atmosphere and the surface; $\mathcal{I}_{5\lambda}^\downarrow$ is the contribution from the atmospheric emission reflected from the surface and scattered back in the direction $\theta(z)$. Since in the thermal emission spectrum the spectral albedo does not exceed $A_\lambda = 0.1$ for most types of the underlying surface, the contribution of $\mathcal{I}_{5\lambda}^\downarrow$ can be neglected in many cases. The contribution of $\mathcal{I}_{3\lambda}^\downarrow$ is not great, and the aerosol effect on the downward thermal emission transformation is determined by $\mathcal{I}_{1\lambda}^\downarrow$, $\mathcal{I}_{2\lambda}^\downarrow$, $\mathcal{I}_{3\lambda}^\downarrow$.

Tables 2, 3 give the data on spectral radiances of the downward thermal emission at the altitude z = 2 km at viewing angles $\theta = 0^o, 85^o$ for the atmosphere with the temperature of the surface atmospheric layer T = 17°C and the mean tropospheric humidity r = 60-40 % . The optical thickness $\tau_{aerosol} = 1$, for the chemical composition corresponding to the mean-global continental aerosol which contains mineral and industrial aerosol as well as the particles of water solutions. In this case the aerosol has comparable coefficients of absorption and scattering in

TABLE 2

Contribution of the Components $J_{1\lambda}^{\downarrow}$, $J_{2\lambda}^{\downarrow}$, $J_{4\lambda}^{\downarrow}$ ($W/cm^2 sr$) Into the Spectral Radiance of the Downward Thermal Emission $J_{\lambda}^{\downarrow}$ for Different Wavelengths λ in the 2-15 um Spectral Region at the Altitude $z = 2$ km, $\theta = 0°$.

1.94	389 - 9	210- 10	114 - 10	413 - 9	4.2	179 - 4	103 - 5	352 - 6	193 - 4
2.01	477 - 9	408 -10	608 - 10	579 - 9	4.3	222 - 4	121 - 5	419 - 6	228 - 4
2.10	270 - 9	309 -10	385 - 9	689 - 9	4.5	259 - 4	247 - 5	120 - 5	296 - 4
2.20	158 - 9	258 -10	118 - 8	155 - 8	4.7	869 - 5	221 - 5	912 - 5	200 - 4
2.30	115 - 8	180 - 9	248 - 8	381 - 8	4.9	277 - 4	320 - 5	730 - 5	382 - 4
2.55	688 - 7	294 - 8	112 - 8	729 - 7	5.2	638 - 4	501 - 5	264 - 5	714 - 4
2.65	123 - 6	353 - 8	158 - 8	128 - 6	5.5	880 - 4	522 - 5	208 - 5	953 - 4
2.70	161 - 6	427 - 8	197 - 8	167 - 6	6.0	126 - 3	179 - 5	950 - 6	129 - 3
2.90	422 - 6	133 - 7	740 - 8	443 - 6	6.8	187 - 3	439 - 5	223 - 5	194 - 3
3.00	580 - 6	195 - 7	212 - 7	601 - 6	7.5	232 - 3	117 - 4	645 - 5	250 - 3
3.30	158 - 5	803 - 7	108 - 6	177 - 5	8.0	199 - 3	151 - 4	264 - 4	240 - 3
3.40	138 - 5	115 - 6	384 - 6	188 - 5	10.0	110 - 3	126 - 4	790 - 4	202 - 3
3.55	109 - 5	169 - 6	960 - 6	222 - 5	12.0	147 - 3	845 - 5	605 - 4	216 - 3
3.70	115 - 5	202 - 6	160 - 5	295 - 5	13.5	276 - 3	540 - 5	363 - 5	285 - 3
3.90	170 - 5	407 - 6	246 - 5	457 - 5	14.0	265 - 3	398 - 5	274 - 5	272 - 3
4.10	152 - 5	449 - 6	431 - 5	628 - 5	14.8	245 - 3	162 - 5	104 - 5	248 - 3

TABLE 3

Contribution of the Components $J_{1\lambda}^{\downarrow}$, $J_{2\lambda}^{\downarrow}$, $J_{4\lambda}^{\downarrow}$ ($W/cm^2 sr$) Into the Spectral Radiance of the Downward Thermal Emission $J_{\lambda}^{\downarrow}$ for Different Wavelengths λ in the 2-15 μm Spectral Region at the Altitude $z = 2$ km, $\theta = 85°$.

1.94	428 - 9	428 -10	389 -10	510 - 9	4.2	179 - 4	232 - 5	158 - 5	218 - 4
2.01	874 - 9	589 -10	133 - 9	106 - 8	4.3	212 - 4	274 - 5	187 - 5	258 - 4
2.10	128 - 8	456 -10	649 - 9	197 - 8	4.5	290 - 4	304 - 5	289 - 4	349 - 4
2.20	991- 9	316 -10	196 - 8	298 - 8	4.7	268 - 4	161 - 5	105 - 4	389 - 4
2.30	545 - 8	210 - 9	300 - 8	956 - 8	4.9	463 - 4	398 - 5	847 - 5	587 - 4
2.55	688 - 7	829 - 8	605 - 8	831 - 7	5.2	673 - 4	765 - 5	608 - 5	810 - 4
2.65	123 - 6	118 - 7	930 - 8	144 - 6	5.5	880 - 4	106 - 4	752 - 5	106 - 3
2.70	161 - 6	144 - 7	116 - 7	187 - 6	6.0	126 - 3	506 - 5	407 - 5	135 - 3
2.90	430 - 6	332 - 7	195 - 7	493 - 6	6.8	187 - 3	117 - 4	906 - 5	208 - 3
3.00	661 - 6	380 - 7	432 - 7	742 - 6	7.5	235 - 3	207 - 4	164 - 4	272 - 3
3.30	200 - 5	134 - 6	178 - 6	231 - 5	8.0	263 - 3	166 - 4	221 - 4	302 - 3
3.40	267 - 5	163 - 6	456 - 6	329 - 5	10.0	310 - 3	946 - 5	405 - 4	360 - 3
3.45	343 - 5	184 - 6	119 - 5	480 - 5	12.0	306 - 3	901 - 5	238 - 4	339 - 3
3.70	424 - 5	220 - 6	206 - 5	652 - 5	13.5	276 - 3	705 - 5	646 - 5	289 - 3
3.90	636 - 5	346 - 6	303 - 5	974 - 5	14.0	264 - 3	584 - 5	525 - 5	275 - 3
4.10	755 - 5	373 - 6	524 - 5	132 - 4	14.8	245 - 3	441 - 5	362 - 5	253 - 3

the region of most important transparency window 8-13 μm, and the effect of the aerosol on $\mathcal{I}_\lambda^\downarrow$ is most strongly pronounced.

Since the elongation of the phase function decreases with wavelength, the directional re-distribution of the thermal emission radiance in the 8-13 μm window should be more marked. If in the shortwave ($\lambda < 3$ μm) spectral region the contribution of $\mathcal{I}_{2\lambda}^\downarrow$ and $\mathcal{I}_{4\lambda}^\downarrow$ is small, then when the wavelength grows, their contribution to the total radiance $\mathcal{I}_\lambda^\downarrow$ increases considerably and becomes comparable with $\mathcal{I}_{1\lambda}^\downarrow$, and in the transparency window $\mathcal{I}_{3\lambda}^\downarrow$ may exceed $\mathcal{I}_{1\lambda}^\downarrow$.

Calculations made for the models of the continental and marine aerosol as well as the dust-storm aerosol confirmed the main feature of the aerosol effect on the spatial structure of the downward thermal emission: the aerosol is responsible for a marked directional re-distribution of $\mathcal{I}_\lambda^\downarrow$. In this case $\mathcal{I}_\lambda^\downarrow$ increases at $\theta > 60^\circ$ and decreases at $\theta > 80^\circ$, and variations of $\mathcal{I}_\lambda^\downarrow$ with varying θ decrease. Scattering is responsible for smoothing out the emission spatial structure.

Calculations have shown that the absorption mechanism affects greatly the structure and amount of $\mathcal{I}_\lambda^\downarrow$ in the arid and subarid zones, in conditions of dust storms, and over the regions with a high concentration of the industrial aerosol. In the case of the marine aerosol, the effect of the absorption mechanism is less pronounced in high humidity conditions ($r > 80$ %) over seas and oceans, when a large-particle fraction of sea salt solutions contributes to the aerosol scattering.

With increasing altitude the aerosol concentration decreases on the average. However, in this case the atmospheric density decreases too. One may expect that the role of aerosol in the radiation regime and in the upper atmosphere remains significant, and at altitudes exceeding 50 km the aerosol effect on radiances $\mathcal{I}_\lambda^{\uparrow\downarrow}$ may increase due to a temperature difference between a gaseous medium and aerosol. Calculations performed by Fiocco and Grams (1976) have shown that at altitudes more than 60 km the aerosol particle temperature may exceed that of the environmental gas by 30-100K due to the solar radiation absorption. The effect of temperature difference on $\mathcal{I}_\lambda$ is pronounced most strongly in the zone of horizon, since the optical thickness of the aerosol increases with increasing zenith angle more rapidly than the optical thickness of gaseous components.

A Cloudy Atmosphere

Calculations of spectral radiance $\mathcal{I}_\lambda^{\downarrow\uparrow}$ in a cloudy atmosphere were performed for different types of cloudiness and its vertical structure, with cloud tops varying from 2 km to 12 km. Figures 6, 7, 8 show the spectra of $\mathcal{I}_\lambda^\uparrow$ for several observation heights in the atmosphere and viewing zenith angles.

In the case of the upward emission the clouds screen the emission of the Earth's surface and the lower atmosphere, and $J_\lambda^\uparrow$ decreases in transparency windows, while in the bands of strong absorption $J_\lambda^\uparrow$ either remains constant or varies weakly. The cloudiness smooths significantly the spectral structure of emission, and the higher are the clouds, the less is the angular dependence of $J_\lambda^\uparrow$ in transparency windows. If below the observation height the vertical temperature profile is inversional, then the behaviour of $J_\lambda^\uparrow(z, \theta)$ depends significantly on cloud top height, z_0, selected spectral interval, and atmospheric stratification. $J_\lambda^\uparrow$ varies stronger in strong-absorption bands (4.1-4.6; 5-7; 14-17 μm), where the emission of the Earth's surface and the lower atmosphere is absorbed, and radiative contrasts at cloudy/clear atmosphere transition show themselves weakly. In transparency windows, radiative contrasts at the cloudy/clear atmosphere transition are much lower at large viewing zenith angles. Attention should be paid to characteristic peaks of the outgoing thermal emission, which show themselves at large zenith angles in spectral regions of strong absorption bands determined by the emission of a high temperature inversional atmospheric layer at altitudes 40-50 km (Fig. 8).

The clouds increase the downward emission, $J_\lambda^\downarrow$, in the sub-cloud atmosphere in the spectral intervals corresponding to the atmospheric transparency windows. In the spectral intervals with strong atmospheric absorption, the effect of cloudiness either is absent or shows itself weakly. Particularly great is the effect of cloudiness on the radiance $J_\lambda^\downarrow$ at small zenith angles in the adjacent-to-clouds atmospheric layer, and the cloudy/clear atmosphere transition is followed by considerable radiative contrasts.

Spatial-Temporal Variability and Spectral Structure of the Thermal Emission Field for Mars

As to diversity of climatic conditions, the atmosphere of Mars is close to that of Earth. However, in the actively emitting layer of the Martian atmosphere, the upper and lower levels of temperature are significantly lower as compared to those on Earth. The latter affects the values of spectral radiances and the ranges of their spatial-temporal variability. Below we shall consider the specific features of the spectral and spatial structures of the thermal emission fields for Mars based on the analysis of the data of theoretical calculations performed for clear and turbid atmospheres of Mars with most contrast vertical profiles of temperature and relative humidity.

As in the case of the Earth's atmosphere, calculations were mainly performed for low spectral resolution. Only for individual altitudes and atmospheric models, calculations were made with high resolution (Δ = 2-3 cm^{-1}) as well. It is characteristic that the basic features of the spectral structure of the thermal emission field show

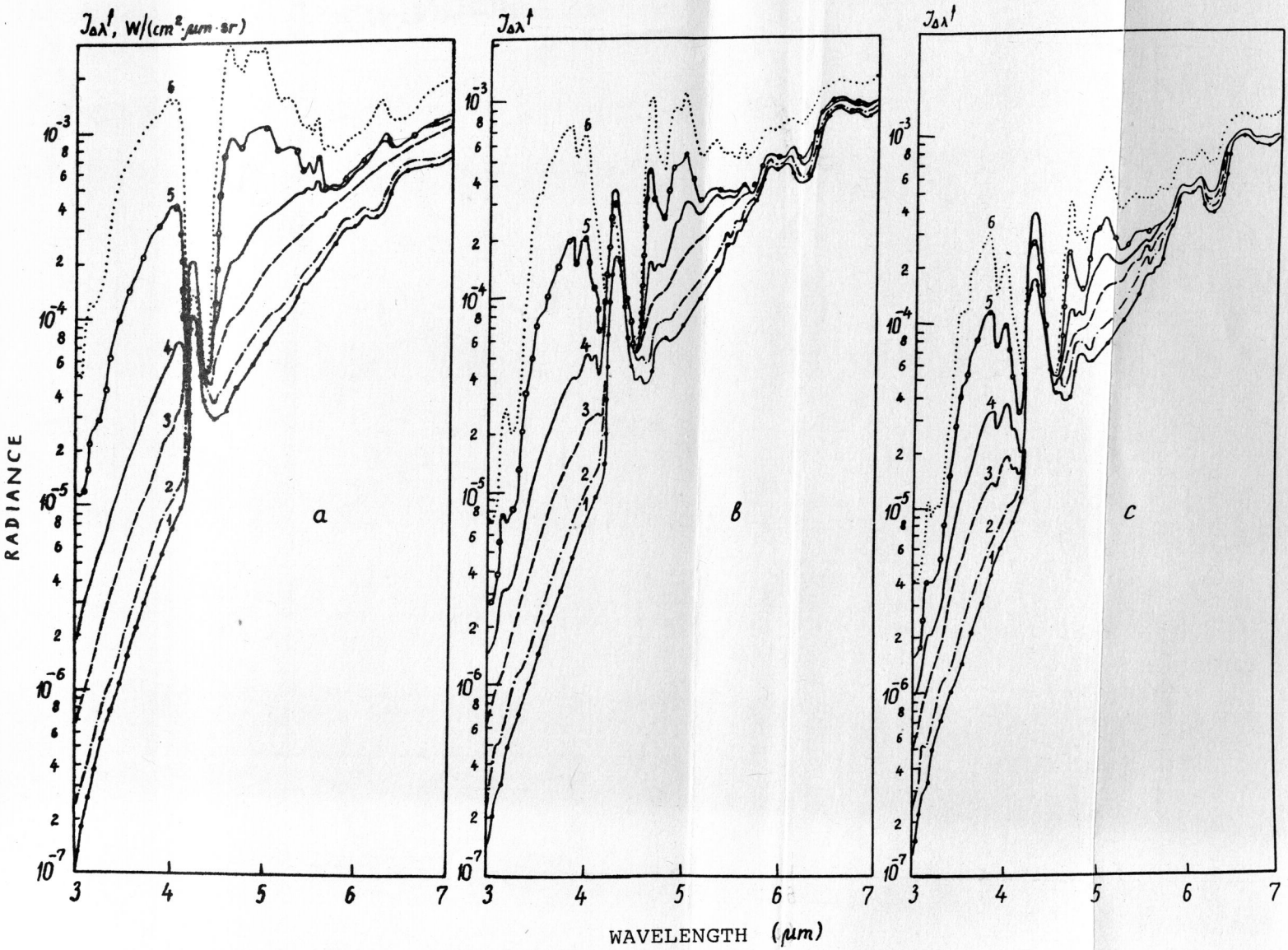

Fig. 6 Spectral radiance of the outgoing thermal emission of the Earth at zenith angles θ (z_0):
a) 0°; b) 85°; c) 90° (z_0 - cloud top height).
1, 2, 3, 4 - atmospheric stratification I with cloud tops at 11.8; 10.2; 8.2; 6 km, respectively;
5, 6 - clear atmosphere for stratifications 6, 12.

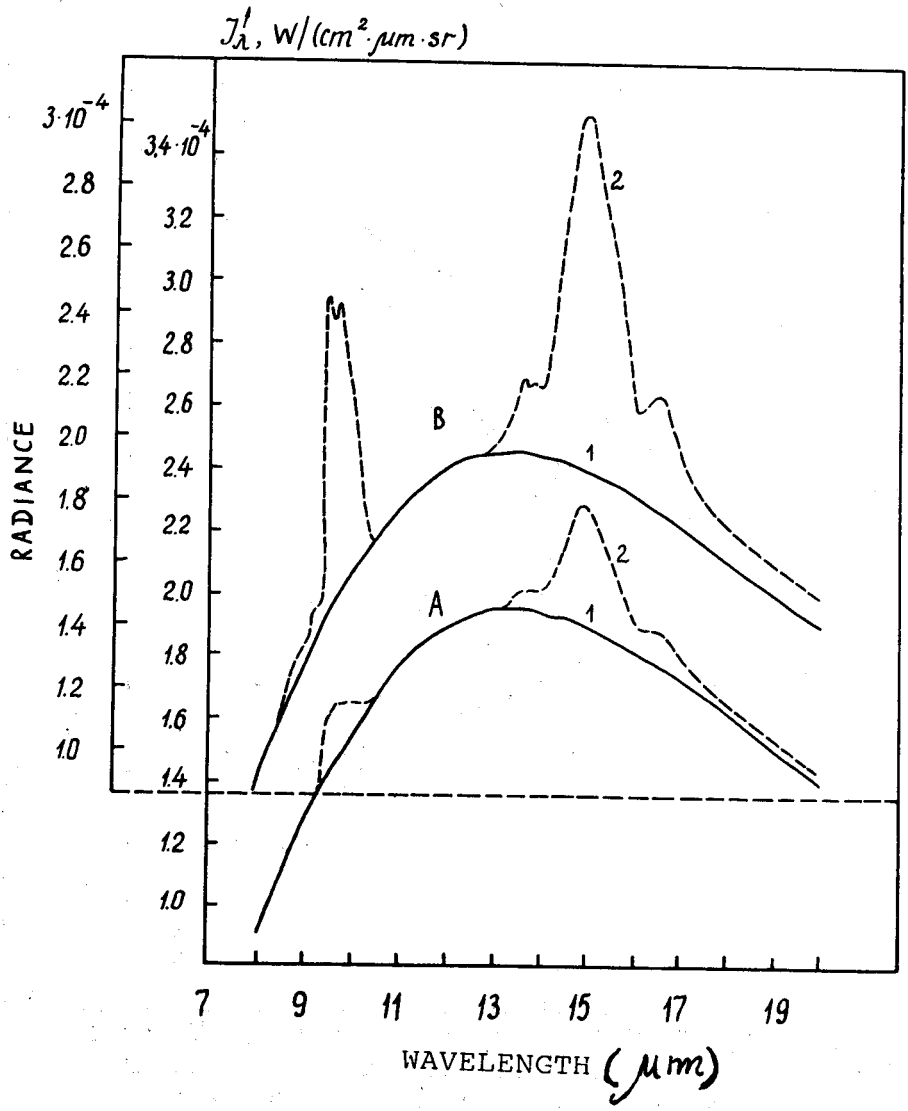

Fig. 7 Spectral radiances of the outgoing (curve 2) thermal emission and upward (curve 1) emission at a level of cloud tops z_o = 11.8 km. Atmospheric stratification 1, zenith angle θ : A - 0°, B - 85°.

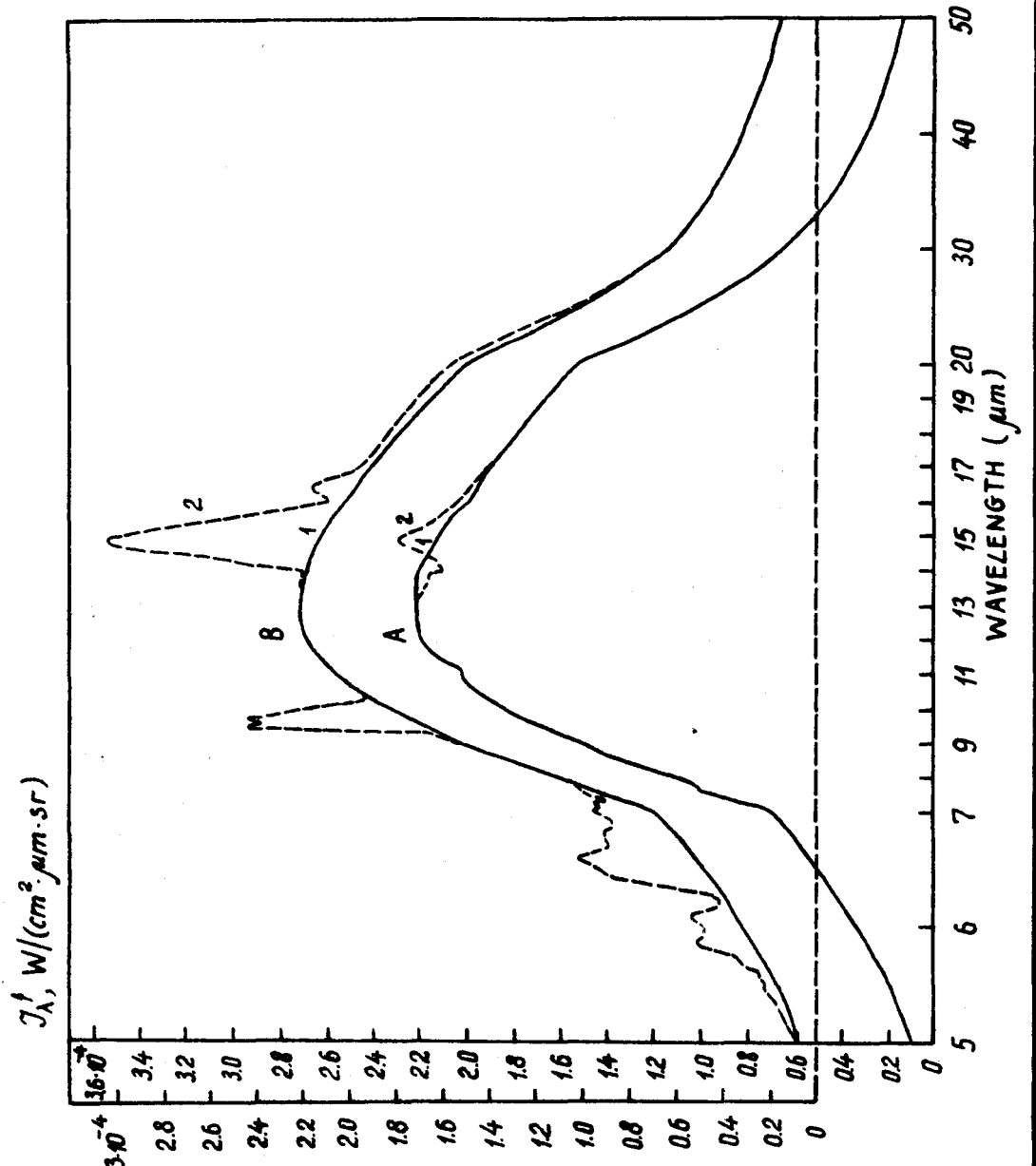

Fig. 8 Spectral radiances of the outgoing (curve 2) thermal emission and upward (curve 1) emission at a level of cloud top z_0 = 10.25 km. Atmospheric stratification 1, zenith angle θ : A - 0°, B - 85°.

themselves also at low resolution Δ = 0.025-0.1 μm. This can be seen in Fig. 9, which shows the spectra of radiative temperature for Mars at zenith angles 0^{o} and 80^{o}. The surface temperature was 270K, the vertical temperature profile T(z) was characterized by a negative lapse rate $\partial T/\partial z < 0$. In the atmosphere with a negative temperature lapse rate the radiance decreases in the absorption bands of the Martian atmosphere. Spectral radiances $\mathcal{J}_{\lambda}^{\uparrow}(z, \theta)$ vary most widely with changing zenith angle and altitude in the CO_2 absorption bands 4.3 and 15 μm. This effect leads also to a decrease in radiative temperature when the observational height and zenith angle grow.

As compared to Earth, the atmosphere of Mars is more transparent, therefore, in most transparent spectral regions in the 4.6-9 μm interval, the radiance $\mathcal{J}_{\lambda}^{\uparrow}$ varies weakly with altitude and zenith angle. Spectral intervals with minimum values of $\mathcal{J}_{\lambda}^{\uparrow}$ correspond to the centers of active absorption of emission by the atmosphere: 15, 7.6, 5.2, 4.8, 2.7 μm - the CO_2 absorption bands.

The atmosphere of Mars is more humid when there is no aerosol. With a maximum total water content ($w\,H_2O$ = 50 μm of precipitable water), the outgoing emission decreases by not more than 20 % in the spectral regions of the strongest absorption within the 6.3 μm band. However, at zenith angles $\theta > 85^{o}$, these differences may reach a factor of 0.5. Since most fraction of water ($\sim$ 80 %) is contained in the surface atmospheric layer 0-3 km, the above-lying atmospheric layers do not practically transform the upward emission in the 6.3 μm water vapour band. Water vapour transform significantly the upward emission in the rotational spectral region $\lambda > 20$ μm.

In the case of the vertical temperature profile with clearly pronounced inversion, the spectra of the outgoing emission have an emissive character, when the bands of atmospheric emission (4.3, 9.6, 10.4, 15 μm) are clearly seen against the total emission (Fig. 10).

Radiance spectra of the downward thermal emission for Mars are described in detail by Kondratyev and Moscalenko (1977), and Moscalenko (1975). Therefore, we shall only mention the basic conclusions. Spectral radiance $\mathcal{J}_{\lambda}^{\downarrow}$ strongly depends on altitude z and zenith angle θ and reflects spectral variations of absorptivity with clearly identified absorptions bands of CO_2 (4.3, 4.8, 5.2, 7.6, 9.4, 10.4, 15 μm), as well as the fundamental (6.3 μm) and rotational ($\lambda > 20$ μm) bands of water vapour. Maximum values of $\mathcal{J}_{\lambda}^{\downarrow}$ correspond to the centers of absorption bands, and minimum values of $\mathcal{J}_{\lambda}^{\downarrow}$ correspond to atmospheric transparency windows. In the case of a complicated vertical temperature profile, a rather complicated pattern is observed of the spectral and spatial structure of the downward emis-

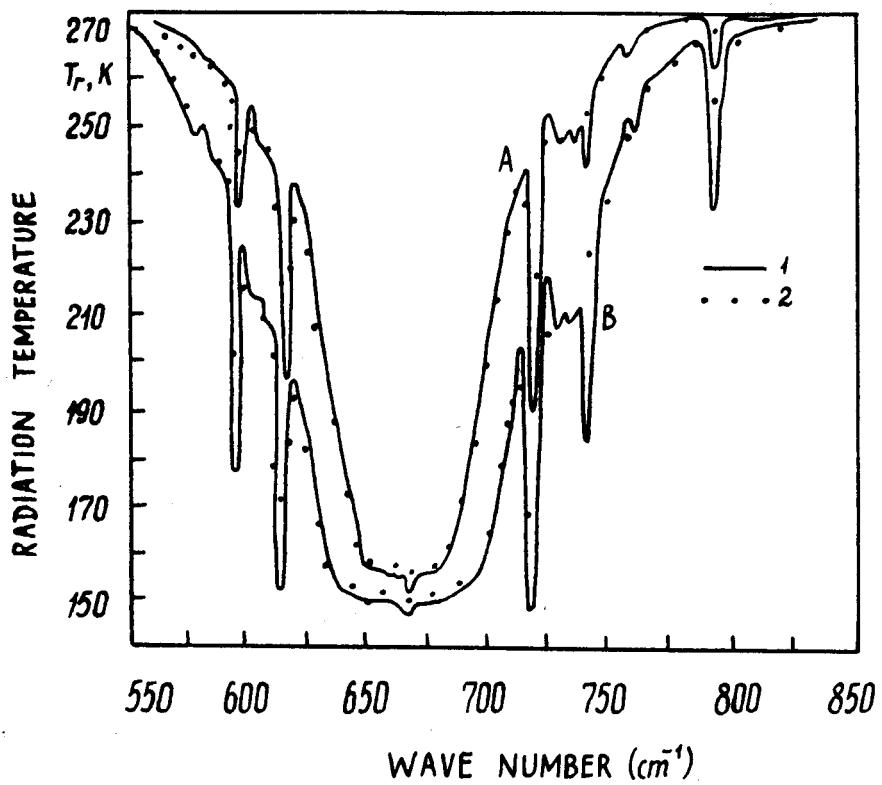

Fig. 9 Spectral radiation temperature T_r of the 15 μm CO_2 absorption band for the outgoing thermal emission of Mars at zenith angles θ : A - 0^o, B - 85^o.

sion in spectral regions with strong absorption bands. Note that in spite of small amounts of water in the Martian atmosphere, its effect (in the case of the absent aerosol) on spectral radiances is strong in CO_2 transparency windows.

In the turbid atmosphere of Mars the amount of water decreases almost by an order of magnitude (due to absorption by the Martian dust particles), and in these conditions its effect on the transformation of the thermal emission field is small. But the effect of aerosol on radiative characteristics of the Martian atmosphere during a dust storm becomes very strong. In contrast to Earth, the Martian aerosol is homogeneous as to its chemical composition, but exhibits broad spatial-temporal variability in concentration and size distribution. Strong absorption bands in the spectral region $\lambda > 7$ μm are characterized by a considerable effect of aerosol on radiative regime of the planet Mars. The fraction of the solar energy reaching the surface and, consequently, its temperature decrease due to attenuation. At the

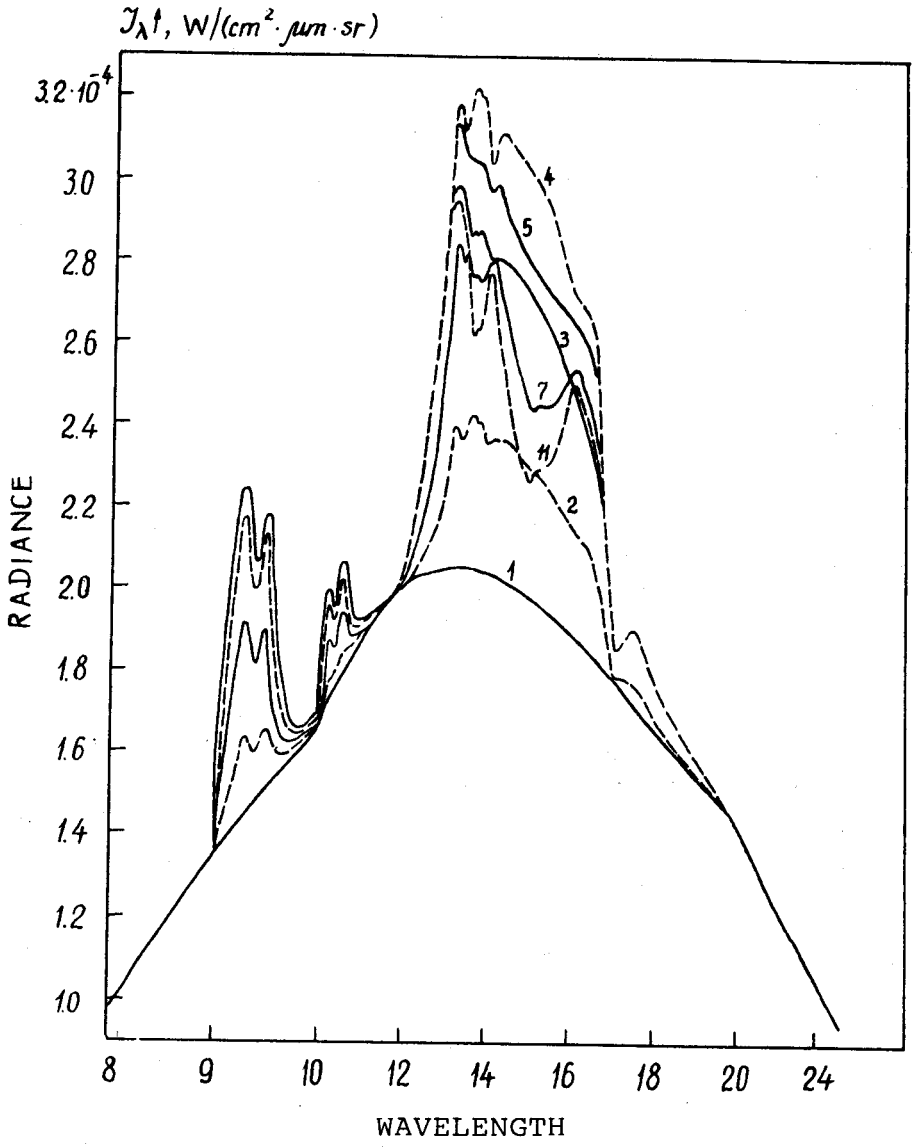

Fig. 10 Spectral radiance of the upward thermal emission of Mars in the 8-25 μm spectral region for inversional temperature profile at altitudes z, km: 1 - 0.1; 2 - 4; 3 - 8.6; 4 - 14; 5 - 18.6; 6 - 25; 7 - 44.

same time, the aerosol, while absorbing the solar energy, warms the atmospheric layers at altitudes 5 to 20 km, smoothing the vertical temperature profile. Since the atmosphere of Mars is not so dense, the conditions may occur in the noon period

for temperature difference between aerosol particles and atmospheric gas. This leads to intensification of generation of the thermal emission in the bands of aerosol absorption.

Calculations of the thermal emission fields for different models of aerosols, revealed considerable effect of aerosol size distribution on radiances of the upward $J_\lambda^\uparrow$ and downward $J_\lambda^\downarrow$ emissions. The best agreement between calculated and measured spectral emissions was obtained for γ - size distribution with parameters $\alpha = 2$, $\beta = 9$, $\gamma = 0.5$. This result was later confirmed by Toon, Pollack, Sagan (1977) who compared the calculated spectra of $J_\lambda^\uparrow$ and those measured from Mariner 9 for several atmospheric conditions.

Spatial variability of the radiances of the downward and upward emissions in the regions of radiation absorption by atmospheric aerosol is similar to that of $J_{\Delta\lambda}^{\downarrow\uparrow}$ for spectral regions with molecular absorption bands in conditions of a clear atmosphere. If the temperature lapse rate is negative, then the stronger is aerosol absorption, the more decreases the radiance of the upward emission $J_\lambda^\uparrow$ with increasing height, and in the spectra of $J_\lambda^\uparrow$ "aerosol pits" are observed, the depth of which increases with increasing height and zenith angle. In the case of the inversional vertical temperature profile, emission bands of aerosol may be observed in the spectra of the upward and outgoing emission.

With growing zenith angle, radiance of the downward emission increases in spectral regions with aerosol absorption bands, except for a very dense aerosol cloud with an optical thickness $\tau_{\text{aerosol}} = 3$, and the inversional temperature profile. In the 5.4-7 μm spectral region corresponding to a transparency window, the radiance $J_\lambda^\uparrow$ increases several times due to backscattering of the upward emission of Mars.

Spectral Structure and Spatial Distribution of the Thermal Emission Fields in the Atmosphere of Venus

Calculations of the spectral and spatial distribution of the downward and upward emission in the atmosphere of Venus were carried out with due regard to the temperature effect on the spectral tranmission function for continuum and pressure-induced absorptions. The calculation technique considered absorption of emission by CO_2, water vapour, CO, HCl, HF, CH_4, NH_3, SO_2, N_2, O_2, and aerosols. Calculations performed for 12 models of the Venusian atmosphere with different cloud tops and bottoms and concentration of aerosols made it possible to determine basic features of the spectral structure and spatial variability of the upward and downward emission fields in the atmosphere of Venus.

The atmosphere of Venus is more opaque than those of Mars and Earth, and its opacity grows toward the surface of the planet. Due to this fact, the sub-cloud atmosphere of Venus can be considered as an absolute black emitting medium in many spectral intervals with strong CO_2 absorption bands: emission radiance is practically equal to spectral brightness of the blackbody at a temperature T(z) in the observation point z . Spectral radiance of the downward and upward emission for the spectral regions 1.9-2.2; 2.5-3.2; 3.7-5.6; 6-30 μm is independent of the observation direction. In the absence of water vapour, CH_4, NH_3, CO, HCl in the atmosphere of Venus, the spectral structure of $J_\lambda^{\downarrow\uparrow}$ more pronounced at altitudes 30-40 km, shows itself only in transparency windows 1.9; 2.2-2.5; 3.2-3.6; 5.6-6 μm. At $z < 10$ km the atmosphere of Venus can be considered as a black emitter, at least in the interval $\lambda > 1.9$ μm.

The presence of water vapour, CH_4, NH_3 leads to a considerable increase of atmospheric opacity on Venus in CO_2 transparency windows. If concentrations of $C(NH_3)$, $C(CH_4)$ and $C(H_2O)$ are more than 10^{-7}, the sub-cloud atmosphere of Venus can be considered as a black emitter, and spectral radiances of both downward and upward emissions decrease with height. Since the temperature field varies weakly with the observation point in contrast to Earth and Mars, the thermal emission radiances also vary weakly with time, season and observation point.

Calculations have shown that the thickness of the cloud layer inside of which the outgoing emission is formed, constitutes 5-7 km for selected cloud models. The aerosol layer which has an absorption optical thickness $\tau_{aa} \approx 1$, contributes mostly to emission. Since τ_{aa} varies with wavelength, the radiation temperature which corresponds to the outgoing emission undergoes important spectral variations (Fig. 11).

Veneras 9 and 10 measured the radiances of the outgoing emission of Venus in the spectral regions 8-13 and 18-28 μm. Analysis of the results carried out by Keldysh (1977) has shown that the radiation temperature of the dark side of Venus is 244K, and that of the bright side 233-234K. One of possible reasons of this difference is an increase in cloud height due to intensified turbulent motions (convective flows) caused by heating of atmospheric layers by solar shortwave radiation. These vertical flows, on one hand, raise a radiation-absorbing substance to altitudes 3-4 km, and on the other hand, they promote formation of an aerosol layer of a heightened concentration in the zones of strong turbulent mixing. Note that the Mariner 10 data obtained mainly for the night side, gave a higher radiation temperature $T_r = 255$K in the 45 μm spectral region. The latter is determined by increasing contribution of emission in this spectral region from deeper aerosol layers. This is verified by theoretical calculations (Fig. 11). In deep layers the spectral radiances of the downward and upward emission are close to the spectral brightness of an absolute blackbody at a temperature of the atmosphere at observation height.

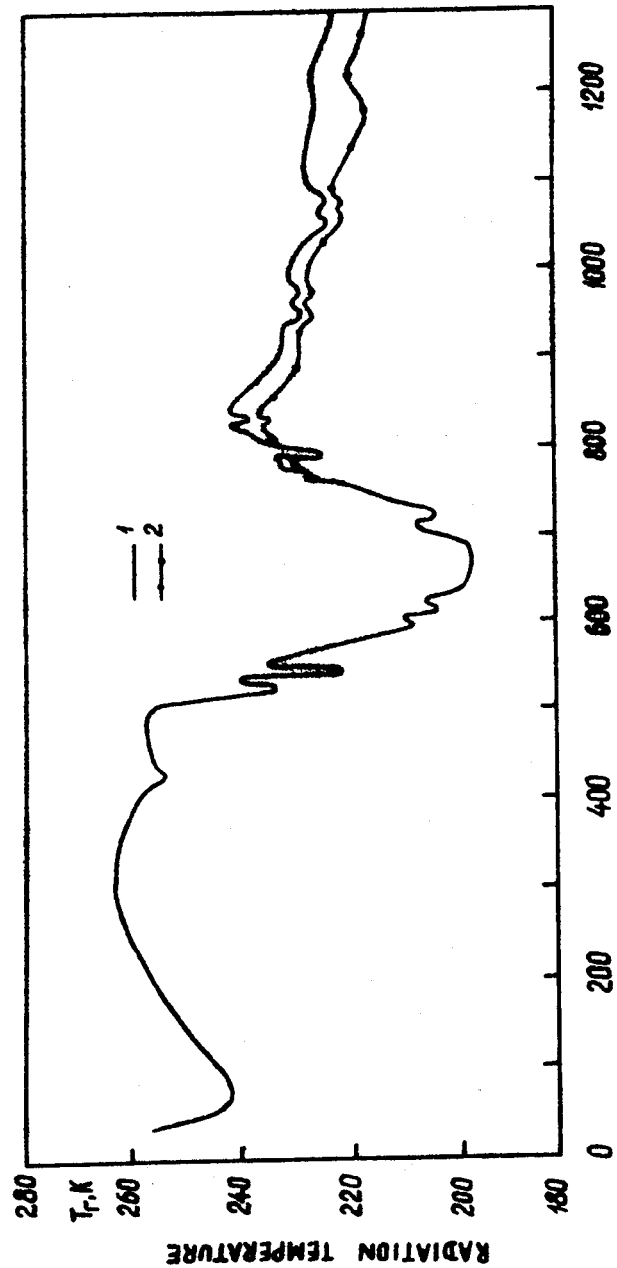

Fig. 11 Spectral radiation temperature T_r for the outgoing thermal emission of Venus for 1-modal (1) and 2-modal (2) microstructure of the upper cloud layer.

Only in a pure CO_2 atmosphere in the spectral regions 5.6-6.5 μm, 8-9 μm, 11-12 μm, 30-50 μm the values of $\mathcal{J}_d^{\downarrow\uparrow}$ ($\mathcal{J}_\lambda^{\uparrow} > \mathcal{J}_\lambda^{\downarrow}$) are different. Practically in the whole spectral region of the thermal emission $\mathcal{J}_\lambda^{\uparrow} \approx \mathcal{J}_\lambda^{\downarrow}$ if the atmosphere contains ammonia and water vapour with a volume concentration of $C \cong 10^{-4}$, in the altitude range 45-60 km. The cloud cover is an important factor regulating the radiative regime of the atmosphere at altitudes more than 40 km. Moscalenko and Zakirova (1975) discussed spectral and spatial structures of the thermal emission field in the above-cloud atmosphere of Venus. Here we shall briefly mention the basic features and peculiarities in $\mathcal{J}_\lambda^{\downarrow\uparrow}$.

The greatest spatial variability of the spectral radiance $\mathcal{J}_\lambda^{\uparrow}$ is observed in the spectral intervals corresponding to strong CO_2 absorption bands, where $\mathcal{J}_\lambda^{\uparrow}$ is minimum. Maximum values of $\mathcal{J}_\lambda^{\uparrow}$ correspond to atmospheric transparency windows 5.2; 5.6; 8.3; 11.5 μm. An increase in humidity transforms significantly the spectral and spatial structures of the outgoing emission only in the interval 5.4-7.8 μm. Addition of a minor component SO_2 leads to a decrease in $\mathcal{J}_\lambda^{\uparrow}$ in spectral intervals within strongest absorption bands 4; 7; 5; 8.8; 20 μm. SO_2 may substantially affect the transformation of the up- and downward emission fields in the above-cloud atmosphere of Venus. An increase in cloud-top height leads to a decrease in $\mathcal{J}_\lambda^{\uparrow}$ in transparency windows of the Venusian atmosphere.

Variations in the Venusian atmosphere's stratifications affect less the values of $\mathcal{J}_\lambda^{\uparrow}(z)$ as compared to the atmospheres of Earth and Mars. Radiance spectra for $\mathcal{J}_\lambda^{\uparrow}(z)$ in the Venusian atmosphere are more homogeneous as to spectral and spatial structures and are less subjected to temporal variations.

On the whole, the spectral structure of the downward emission reflects also spectral variations of atmospheric absorptivity. For atmospheric stratifications with a negative temperature lapse rate $\partial T/\partial z$, $\mathcal{J}_\lambda^{\uparrow}$ decrease with increasing z . Variability of $\mathcal{J}_\lambda^{\uparrow}$ increases with increasing absorptivity of the atmosphere. Minimum radiances $\mathcal{J}_\lambda^{\uparrow}$ correspond to transparency windows, and maximum $\mathcal{J}_\lambda^{\downarrow}$ to the centers of absorption bands. As z increases, the structure of the downward emission shows itself more clearly, and the dependence of $\mathcal{J}_\lambda^{\downarrow}$ on the zenith angle becomes more substantial. The presence and concentration of minor components such as H_2O, NH_3, SO_2, CH_4 affect greatly the radiances of the downward emission in the above-cloud atmosphere of Venus. In connection with this, determination of their concentrations is important for estimation of radiative regime in both the above-cloud and sub-cloud atmosphere of Venus.

Spectral and Spatial Structure of the Thermal Emission in the Sub-Cloud Atmosphere of Jupiter

Information on composition and vertical profiles of temperature obtained on the basis of ground-based observations, from automatic interplanetary stations, has made it possible to construct more or less real models of the vertical structure of the above-cloud atmosphere of Jupiter. Based on the models of the vertical temperature profile by Cook (1973) and Orton (1975) and of the atmospheric chemical composition, the authors performed detailed calculations of spectral and spatial distributions of the thermal emission fields in the above-cloud atmosphere with account of molecular absorption by NH_3, CH_4, C_2H_2, C_2H_4, C_2H_6, as well as H_2 - H_2, H_2 - He collision-induced absorption.

Note, that such minor components as C_2H_2, C_2H_4, C_2H_6 play a significant role in the thermal emission transfer only in the upper atmosphere of Jupiter at more than 70 km above clouds. In this connection, it is most important to take into account the absorption band ν_5 C_2H_2 centered at 729.1 cm^{-1}, the bands ν_7 and ν_{12} C_2H_4 centered at 949.2 and 1443.5 cm^{-1}, the bands ν_8 and ν_9 C_2H_6 centered at 1486 and 820.8 cm^{-1}. The absorption bands for methane, acetylene, ethylene and ethane play a decisive role in the radiative regime of the upper atmophere of Jupiter at altitudes more than 90 km. The role of water vapour in the radiative regime of Jupiter's atmosphere is rather small.

Figure 12 shows the data on the spectral radiance of the upward thermal emission on Jupiter at different zenith angles from 0^o to 90^o at altitudes 47 and 88 km above clouds for stratification I of the atmosphere.

Characteristic features of formation of the thermal emission spectra in the atmosphere of Jupiter are first of all explained by the spectral structure of the transmission function: strong absorption of the i.r. radiation in rotational-vibrational bands of atmospheric NH_3 and CH_4 and pressure-induced H_2 bands. There is no doubt that NH_3 plays a decisive role in the thermal regime of Jupiter like water vapour in the atmosphere of Earth. In the interval from 2 to 200 μm the atmosphere of Jupiter is practically opaque in the vertical, except for a narrow spectral interval near $\lambda = 4.5$ μm. In connection with this, the spectral structure of the downward $J_\lambda^\downarrow$ and upward $J_\lambda^\uparrow$ thermal emissions below 50 km is weakly pronounced. In the 5-25 μm spectral region $J_\lambda^{\uparrow\downarrow}$ do not depend on zenith angle. In the 4.3-5.3 μm region, minimum $J_\lambda^\downarrow$ and maximum $J_\lambda^\uparrow$ are observed due to weak radiation absorption in the atmosphere. With an altitude increasing to 50 km, $J_\lambda^{\downarrow\uparrow}$ decrease, which is explained by a negative temperature lapse rate. In the 20-30 μm region the spectral structure of $J_\lambda^{\downarrow\uparrow}$ and its dependence on zenith angle shows itself practically at all the latitudes, and as the altitude grows, $J_\lambda^{\downarrow\uparrow}(z, \theta)$ varies strongerly depending on θ.

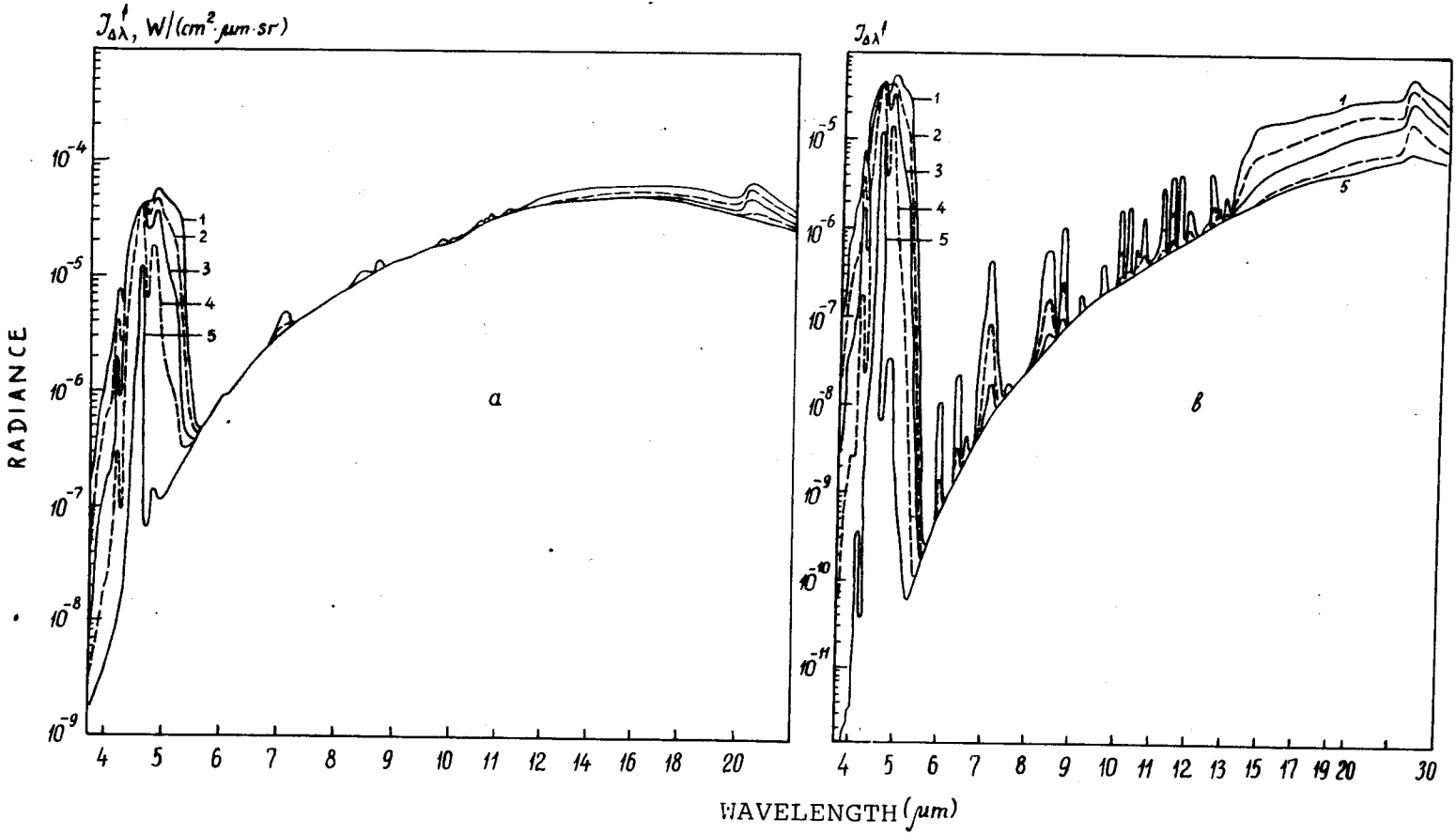

Fig. 12 Spectral radiance for the upward thermal emission in Jovian atmosphere in the 4-30 μm region at different viewing angles θ : 1 - 0°, 2 - 60°, 3 - 75°, 4 - 85°, 5 - 90°. Altitudes z, km: a - 47, b - 88.

Above 50 km dependences of $\mathcal{J}_\lambda^{\downarrow\uparrow}(\theta)$ show themselves at all the altitudes. In the spectra of the upward emission the absorption bands are clearly seen, and in the spectra of the downward emission the NH_3 emission bands 2, 2.3, 3.2, 3.7, 6.3 μm and CH_4 2.3, 3.3, 7.6 μm. In connection with great temperature lapse rate, spectral radiances $\mathcal{J}_\lambda^{\uparrow}$ exhibit wider variations with changing altitude than in the atmospheres of Earth, Mars and Venus.

Analysis of calculation results has shown that on Jupiter, like on Earth, Venus and Mars, the atmospheric temperature contrasts play a decisive role in the formation of the upward emission fields, while variations in concentration of radiation absorbing components affect weakerly the radiation contrasts (as compared to temperature).

An increase in cloud top height should be followed by decreasing of temperature at the level of the cloud top. This leads to a decrease in radiances of the upward emission in atmospheric transparency windows 4.7 and 17 μm. In strong absorption bands, variations in cloud top height do not affect radiative contrasts of the upward emission in the atmosphere.

It is interesting to evaluate the effect of the aerosol haze at an altitude of 25 km above clouds on the values of $\mathcal{J}_\lambda^{\downarrow\uparrow}$. With this aim in view, characteristics of Jupiter's aerosol haze were calculated, the particles of which were assumed to be water ice and NH_3. Radiances of $\mathcal{J}_\lambda^{\downarrow\uparrow}$ were calculated for the model of a homogeneously dense atmospheric haze with an optical thickness $\tau_o = 0.5$ at a wavelength $\lambda = 0.55$ μm. In all the cases, the contribution of the aerosol haze to values of $\mathcal{J}_\lambda^{\downarrow\uparrow}(z, \theta)$ did not exceed 1% in the 5-15 μm spectral region. The latter is caused by strong emission absorption by atmospheric gases in the altitude range where the haze is observed. However, in the 17-25 μm spectral region, the effect of aerosol may lead to a decrease of radiance $\mathcal{J}_\lambda^{\uparrow}$ down to 5-7% and an increase of $\mathcal{J}_\lambda^{\downarrow}$ to 10-20 %. The latter confirms the necessity of consideration of the aerosol haze effect in remote sounding of the vertical structure of Jupiter's atmosphere.

Radiative Heat Flux Divergences and Vertical Profiles of Radiative Temperature Variations in Planetary Atmospheres

Here we shall compare the data on total radiative heat flux divergences and radiative temperature change in different climatic conditions of Earth, Mars, Venus and Jupiter.

The greatest spatial variations of the upward and downward emission are observed in opaque atmospheres with most changing vertical temperature profile. For

opaque atmospheres, the fluxes of downward and upward emissions are close in the strongly absorbing atmospheric layers. Vertical variations are maximum for the fluxes of the upward $F^{\uparrow}(z)$ and downward $F^{\downarrow}(z)$ emission in the atmosphere of Venus. So, for instance, depending on height, $F^{\uparrow}(z)$ varies from 18916 W/m^2 at the surface level to 156.2 W/m^2 for the outgoing emission. In the above-cloud atmosphere of Jupiter, the fluxes $F^{\uparrow}(z)$ vary from 263.2 W/m^2 at the cloud level to 11.76 W/m^2 in an altitude range with minimum temperature. The outgoing thermal emission flux on Jupiter constitutes 13.1 W/m^2. The upward thermal emission flux on Mars undergoes considerable spatial and temporal variations and varies from 401 W/m^2 to 21.8 W/m^2, the widest variations of $F^{\uparrow}$ being determined by changing climatic conditions on the planet. The fluxes of the upward and downward thermal emission on Mars vary considerably depending on time, while diurnal variations of $F^{\downarrow\uparrow}(z)$ in the atmospheres of Venus and Jupiter are small. Radiative vertical gradients in the atmosphere of Mars are much smaller than on Earth, Jupiter and Venus. The terrestrial upward emission fluxes vary depending on climatic zones, season and time from 657 W/m^2 to 120 W/m^2.

The downward thermal emission fluxes in the atmospheres of Mars, Venus, Jupiter vary from almost zero at an altitude of the upper atmospheric boundary to 500 W/m^2, 63 W/m^2, 18900 W/m^2, 258 W/m^2 at the surfaces of Earth, Mars, Venus and at an altitude of the upper cloud boundary on Jupiter.

Figure 13 gives the vertical profiles of radiative temperature variations calculated for some models of the Earth's atmosphere. The structure of the thermal emission fluxes for different spectral intervals was analyzed in detail by Kondratyev and Moscalenko (1977). A substantial dependence of vertical profiles of the downward and upward emission on atmospheric stratification determine considerable height-variations of radiative cooling rates with varying atmospheric states. Vertical profiles of $\partial T(z)/\partial t$ vary with height z depending on atmospheric structure. The terrestrial atmosphere is characterized by increasing radiative cooling rate with an increase in surface temperature. Maximum values of tropospheric cooling are observed for the models of the tropical atmosphere as well as arid and subarid regions. In conditions of a very dust-loaded atmosphere, radiative cooling grows in the upper atmospheric aerosol layers and lowers in the surface atmospheric layers.

The presence of fog intensifies radiative cooling of the surface boundary layer, where $\partial T/\partial t$ may reach $-6 + -20$K/day. Clouds lead to inversion in the profile of radiative temperature change. In particular, cooling in the upper cloud layers is intensified, while weak radiative heating is observed in the sub-cloud atmosphere. In the case of the 2-level cloudiness model, a considerable decrease is observed in cooling of an atmospheric layer between the upper and lower layers of cloudiness.

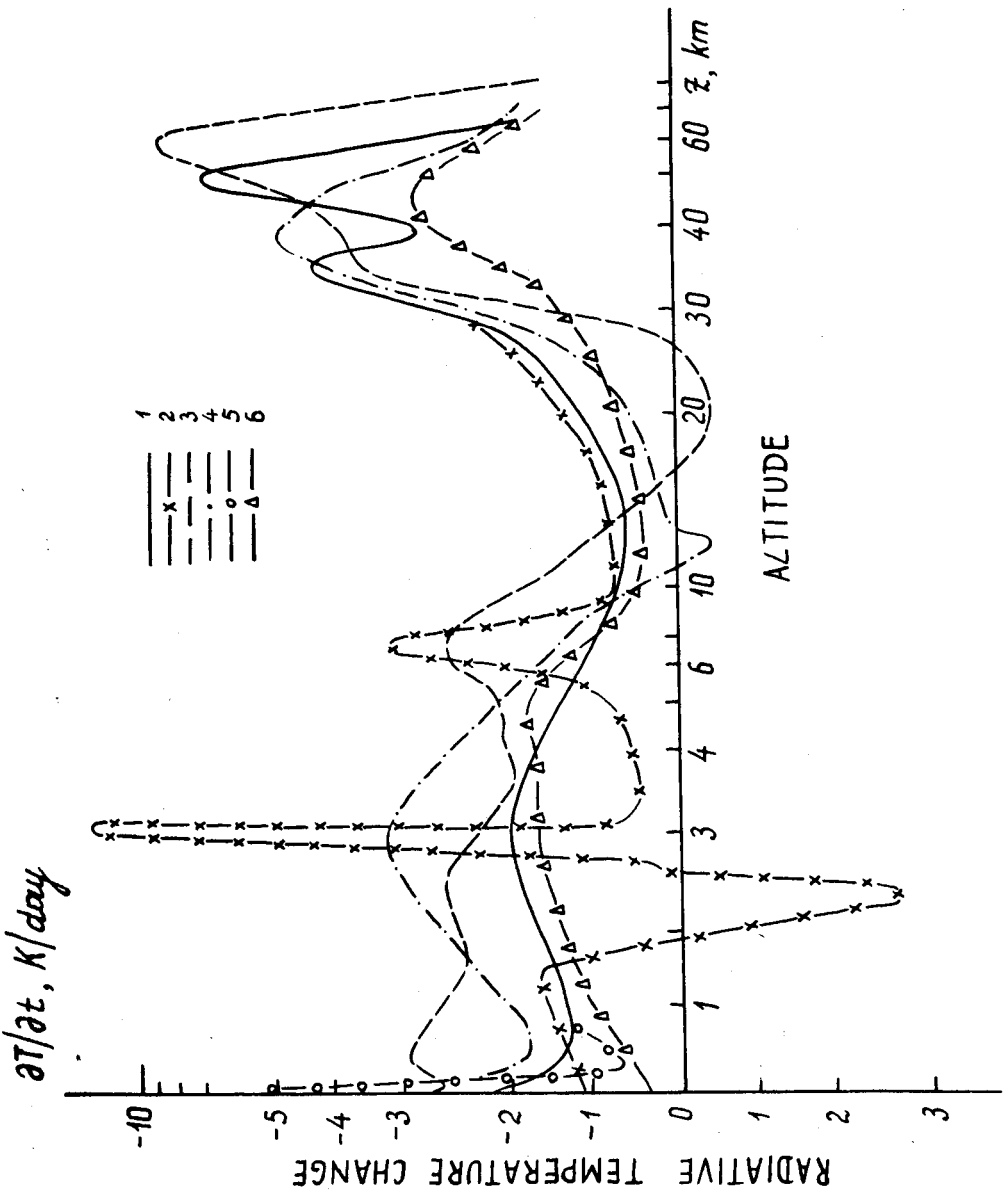

Fig. 13 Vertical profiles of radiation temperature changes for different models of the Earth's atmosphere:

1 - clear atmosphere for model 1; 2 - cloudy atmosphere, Model 1;
3 - clear atmosphere, model 9; 4 - dust storm;
5 - fog in the surface layer; 6 - model 3 of the atmosphere.

Radiative cooling of the stratosphere depends significantly on its humidity and the vertical profile of ozone concentration. Maximum values of $\partial T/\partial t$ are observed at altitudes 40-60 km depending on structural characteristics of the stratosphere. Note, that aerosol-loading of the stratosphere may lead to both radiative cooling and heating depending on optical properties of aerosol. For a mean global atmosphere, the stratospheric aerosol intensifies its radiative cooling. In winter, radiative cooling is less, and for a cold atmosphere with considerable temperature inversion in lower troposphere, heating is observed when $\partial T/\partial t > 0$.

In conditions of the Martian atmosphere, the vertical profiles of atmospheric radiative temperature change differ considerably depending on climatic conditions, especially in the lower 20 km layer of the atmosphere. Figure 14 exemplifies the vertical profiles of the downward and upward emission as well as radiative cooling rates for models 1, 2 of the free CO_2 atmosphere of Mars. Model 1 with a temperature $T(z = 0) = 287K$ and a negative temperature lapse rate $\partial T/\partial z$ characterizes the state of the mid-latitude Martian atmosphere at noon; model 2 with temperature inversion in the 12-18 km altitude range corresponds to nocturnal conditions in mid-latitudes.

Model 1 is characterized by strong radiative cooling of the Martian atmospheric boundary layer at a rate of 4-5°/day, and by radiative heating in the 2-12 km layer at a rate of 1°/day. Above 14 km, with increasing height, the radiative cooling rate increases to 10°/day. Model 2 is characterized by radiative cooling of the atmosphere which increases with increasing altitude in the 0-20 km range, reaching $\partial T/\partial t =$ 8°/day near $z = 20$ km. In the model of the Martian turbid atmosphere with the same vertical temperature profile $T_1(z)$ stronger radiative cooling takes place at altitudes 1 to 10 km, which may reach 5°/day in conditions of a dust storm. For $T_2(z)$ profile, an increase in atmospheric turbidity leads to growing rate of radiative cooling in the 0-10 km layer. Calculations show a substantial effect of humidity on the character of radiative heat exchange in the clear Martian atmosphere, namely, it accelerates radiative cooling at altitudes 0-3 km.

To calculate radiative heat flux divergences in the Venusian atmosphere, the authors developed an optical model of the cloud cover based on the data on its particle size distribution and chemical composition, obtained from Pioneer-Venus results. This model has made it possible to take account of vertical variations of cloud optical properties.

Figure 15 shows the results of calculations of the net flux $F(z)$ for two model cloudiness giving the planetary albedos $\delta_1 = 0.77$ and $\delta_2 = 0.74$. Curves 1, 2 correspond to the basic model of cloudiness and $\delta = 0.77$.

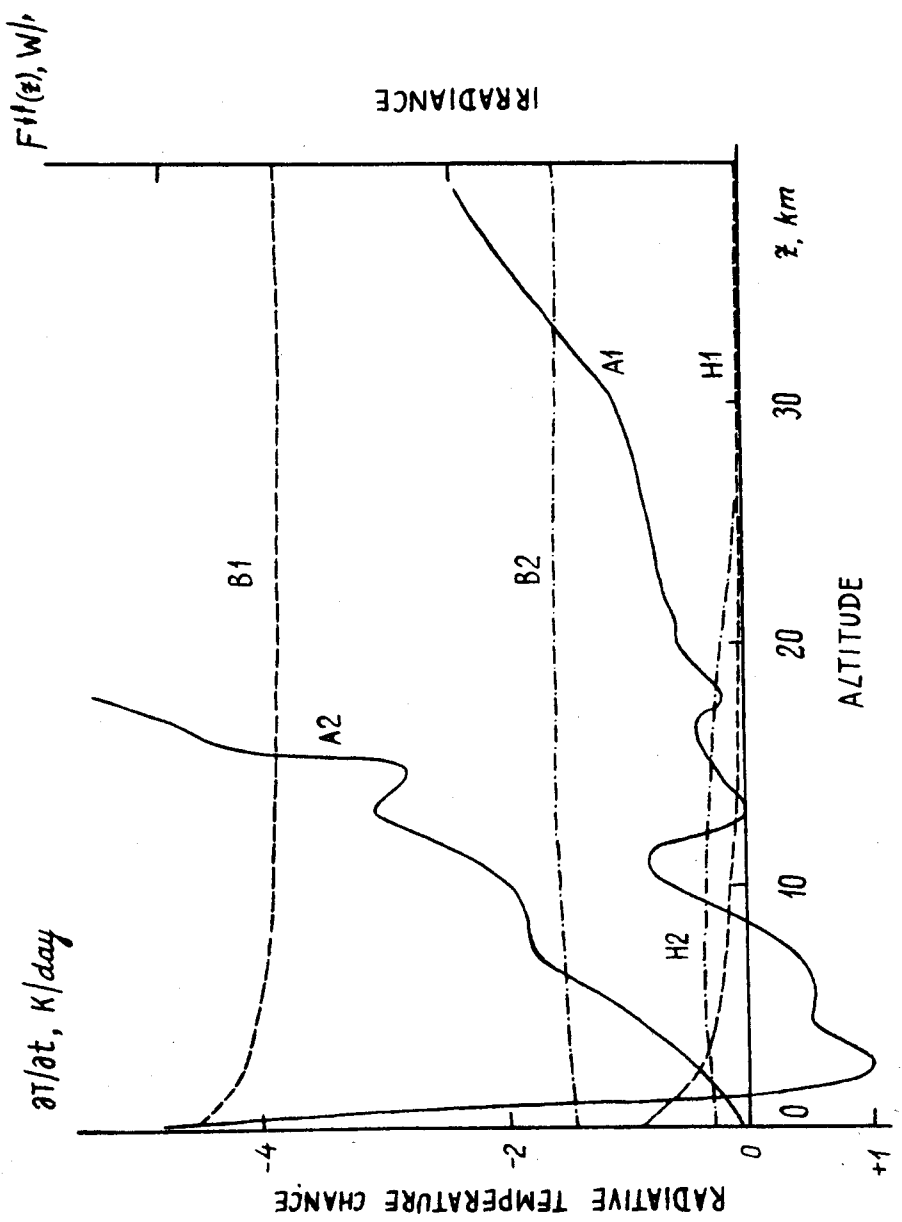

Fig. 14 Height-dependences of the upward B1, B2 and downward H1, H2 thermal emissions and radiation temperature change profile A1, A2 for models 1, 2 of the Martian atmosphere.

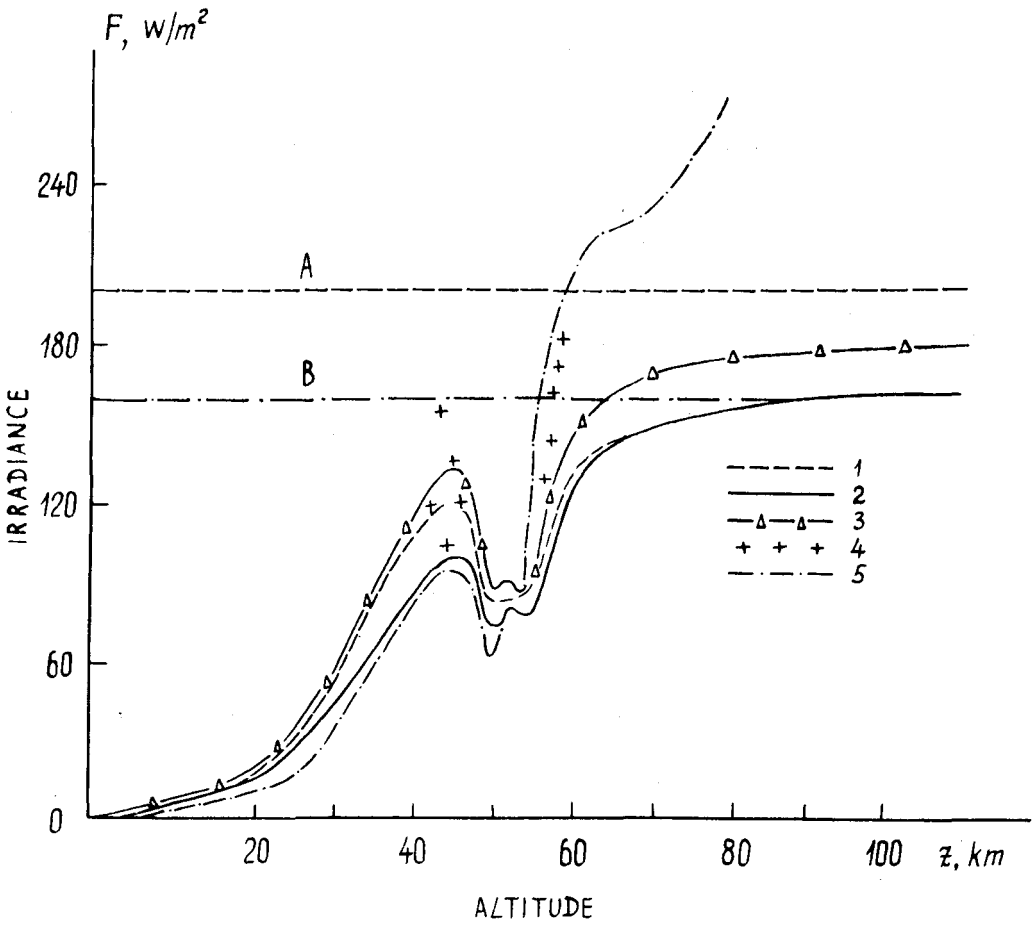

Fig. 15 Profiles of the net radiation flux (F(z) calculated for basic cloud model ($\delta = 0.77$) at water vapour volume concentrations $3 \cdot 10^{-5}$ (1) and $1 \cdot 10^{-4}$ (2); 3 - F(z) calculated for a cloud model with $\delta = 0.74$ and water vapour concentration $3 \cdot 10^{-5}$;
4 - Pioneer-Venus data;
5 - calculations made by Boese and Pollack (1979) with water vapour concentration $1 \cdot 10^{-3}$.

Line A corresponds to a maximum possible solar radiative flux divergence on the planet at $\delta' = 0.7$. Line B corresponds to solar radiative flux divergence at $\delta = 0.77$. Curve 5 due to schematic calculations made by Boese and Pollack (1979) shows inadequate consideration of the optical properties of the Venusian atmosphere. So, for instance, it gives the values of the net flux F (z) exceeding the solar radiative flux divergence even at concentration $C(H_2O) = 1 \cdot 10^{-3}$.

Maximum radiative cooling rate is observed near the altitude range 56-60 km, where $\partial T/\partial z = -2.1$-$3.6$ K/day. In the 56-60 km layer, radiative cooling is followed by heating. In the 45-50 km layer, radiative warming of the atmosphere is observed with maximum value $\partial T/\partial z = 0.9$ K at $z = 49$ km. Beginning from the surface level, radiative cooling rate increases with height from $-3 \cdot 10^{-4}$ K/day (at $z = 0$) to $-1.4 \cdot 10^{-2}$ at $z = 42$ km. At an altitude of 100 km radiative heating reaches 5-7 K/day.

In the atmosphere of Jupiter near a cloud, the radiative temperature change is very small (in the range of pressure variation 3-0.5 atm). Above a level with a pressure $P(z) = 0.5$ atm, the partial pressure of NH_3 is determined by saturation conditions, and at altitudes 30-40 km above clouds, the radiative cooling rate is maximum, reaching 0.015^{o}/day. At altitudes exceeding 60 km, radiative heating takes place with the maximum value $\partial T(z)/\partial t = 0.035^{o}$/day at 90-100 km above clouds.

BIBLIOGRAPHY

BOESE, R. W., F. B. POLLACK, P. M. SILVAGGIO, 1979. First results from the large probe infrared radiometer experiment, *Science, vol. 203,* p.797-802.

COOK, W. S., 1973. Engineering models for Jupiter's troposphere and NH_3-H_2O cloud system. AIAA Pap., No. 129, 7 pp.

FIOCCO, G., G. GRAINS, A. NUGNAI, 1976. Energy exchange and temperature of aerosols in the Earth's atmosphere (0-60 km). *J. Atmos. Sci., vol. 34,* No.7, p.125-134.

HARRISON, A. W., 1976. Atmospheric thermal emission 7-15 μm. *Canad. J. Phys., vol. 54,* No. 14, p. 1442-1448.

KELDYSH, M. V., 1977. Venus exploration with the Venera 9 and 10 spacecraft. *Icarus, vol. 30,* No. 4, p. 605-625.

KNOLLENBERG, R. G., D. M. HUNTEN, 1979. Clouds of Venus particle size distribution measurements. *Science, vol. 203,* p. 792-795.

KONDRATYEV, K. Ya., H. Yu. NIYLISK, R. Yu. NOORMA, 1966. On spectral distribution of radiative heat flux divergences in a free atmosphere. *Izvestia of the USSR Acad. Sci. Physics of the Atmosphere and Ocean, vol. 2,* No. 2, p.121-136 (in Russian).

KONDRATYEV, K. Ya., A. M. BUNAKOVA, 1973. Some specific features of the outgoing thermal emission fields in the atmosphere of Mars and Venus. *Izvestia of the USSR Acad. Sci. Physics of the Atmosphere and Ocean, Vol. 9,* No. 3, p. 247-253 (in Russian).

KONDRATYEV, K. Ya., N. I. MOSCALENKO, 1974. Basic features of the thermal emission fields' formation on Jupiter. *Doklady of the USSR Acad. Sci., vol. 219,* No. 5, p. 1089-1091 (in Russian).

KONDRATYEV, K. Ya., N. I. MOSCALENKO, 1975. Meteorology of Jupiter. *Progress in Science and Technology. Studies in Space, vol. 7,* p. 99-153 (in Russian).

KONDRATYEV, K. Ya., N. I. MOSCALENKO, 1975. Spectral and Spatial structure of the thermal emission field in turbid atmosphere of Mars. *Doklady of the USSR Acad. Sci., vol. 224,* p. 3-20 (in Russian).

KONDRATYEV, K. Ya., N. I. MOSCALENKO, 1975. Analysis of the approximation technique for calculation of the planetary thermal emission fields. *Trudy GGO, issue 363,* p. 3-20 (in Russian).

KONDRATYEV, K. Ya., N. I. MOSCALENKO, 1976. Spectral and spatial structure of the thermal emission in the above-cloud atmosphere of Jupiter. *Izvestia of the USSR Acad. Sci. Physics of the Atmosphere and Ocean, Vol. 12,* No. 2, p. 135-143 (in Russian).

KONDRATYEV, K. Ya., 1976. Meteorology of Venus. *Progress in Science and Technology, Studies in Space, vol. 7,* p. 8-98 (in Russian).

KONDRATYEV, K. Ya., 1977. Meteorology of Planets. Leningrad State Univ. Publ. House, Leningrad, 264 pp. (in Russian).

KONDRATYEV, K. Ya., N. I. MOSCALENKO, V. F. TERZI, 1977. Radiative cooling in the atmospheres of Mars, Venus, Jupiter. *Doklady of the USSR Acad. Sci., vol. 236,* No. 6, p. 1334-1337 (in Russian).

KONDRATYEV, K. Ya., N. I. MOSCALENKO, 1977. Thermal emission of planets. Leningrad, Gidrometeoizdat, 263 pp. (in Russian).

KONDRATYEV, K. Ya., N. I. MOSCALENKO, F. S. YAKUPOVA, 1979. Numerical modelling of the thermal emission transfer in the atmospheres of Venus and Mars. *Doklady of the USSR Acad. Sci., vol. 244,* No. 6, p. 1334-1336 (in Russian).

KUZMIN, A. D., M. Ya. MAROV, 1974. Physics of the planet Venus. Moscow, Nauka Publ. House, 408 pp. (in Russian).

MOROZ, V. I., 1978. Physics of the planet Mars. Moscow, Nauka Publ. House (in Russian).

MOSCALENKO, N. I., 1969. Spectral transmission function for water vapor, CO_2, O_3, N_2O, N_2 components in the atmosphere. *Izvestia of the USSR Acad. Sci. Physics of the Atmosphere and Ocean, vol. 5,* No. 11, p. 1179-1190 (in Russian).

MOSCALENKO, N. I., S. O. MIRUMYANTS, 1970. Calculation technique for spectral absorption of the i.r. radiation by atmospheric gases. *Izvestia of the USSR Acad. Sci. Physics of the Atmosphere and Ocean, vol. 6,* No. 11, p. 1110-1126 (in Russian).

MOSCALENKO, N. I., A. R. ZAKIROVA, 1972. Calculation of the spectral, angular and vertical distribution of the thermal emission field of the surface and atmosphere of Earth, *Izvestia of the USSR Acad. Sci. Physics of the Atmosphere and*

Ocean, vol. 8, No. 8, p. 828-842 (in Russian).

MOSCALENKO, N. I., 1975. Specific features of the spectral and spatial distributions of the thermal emission fields in the atmosphere of Mars. *Izvestia of the USSR Acad. Sci. Physics of the Atmosphere and Ocean, vol. 11,* No. 8, p. 836-844 (in Russian).

MOSCALENKO, N. I., 1975. On the effect of the atmospheric aerosol on spectral and angular distribution of the thermal emission. *Izvestia of the USSR Acad. Sci. Physics of the Atmosphere and Ocean, vol. 11,* No. 12, p. 1254-1262 (in Russian).

MOSCALENKO, N. I., 1975. On the effect of stratified atmosphere and clouds on the spectral, angular and vertical distribution of longwave radiation. *Izvestia of the USSR Acad. Sci. Physics of the Atmosphere and Ocean, vol. 11,* No. 3, p. 245-256 (in Russian).

MOSCALENKO, N. I., A. R. ZAKIROVA, 1975. Calculation of the spectral, angular and vertical distribution of the longwave radiation in the above-cloud atmosphere of Venus. *Izvestia of the USSR Acad. Sci. Physics of the Atmosphere and Ocean, vol. 11,* No. 6, p.599-609 (in Russian).

MOSCALENKO, N. I., 1976. On spectral structure and spatial distribution of the thermal emission in the sub-cloud atmosphere of Venus. *Izvestia of the USSR Acad. Sci. Physics of the Atmosphere and Ocean, vol. 12,* No. 12, p. 1277-1285 (in Russian).

MOSCALENKO, N. I., O. V. ZOTOV, 1977. New experimental studies and specification of the CO_2 spectral transmission function: parameters of Lines. *Izvestia of the USSR Acad. Sci. Physics of the Atmosphere and Ocean, vol. 13,* No. 5, p. 488-498 (in Russian).

MOSCALENKO, N. I. *et al.,* 1978. Study of the absorption spectra for sulphuric gas in the i.r. spectral region. *Izvestia of the USSR Acad. Sci. Physics of the Atmosphere and Ocean, vol. 14,* No. 12, p. 1275-1282 (in Russian).

MOSCALENKO, N. I., F. S. YAKUPOVA, 1978. Solution for the problems of radiation transfer in the atmosphere by computer numerical modelling. In the book: "Abstracts of Papers of the 4th All-Union Symposium on Molecular Spectroscopy of High and Superhigh Resolution", Novosibirsk, p. 178-182 (in Russian).

MOSCALENKO, N. I., Yu. A. ILYIN, S. N. PARSHIN, L. V. RODIONOV, 1979. Pressure-induced absorption of emission in atmospheres. *Izvestia of the USSR Acad. Sci. Physics of the Atmosphere and Ocean, vol. 15,* No. 9, p. 912-919 (in Russian).

MOSCALENKO, N. I., V. F. TERZI, 1979. Construction of closed models of optical characteristics of the atmospheric aerosol. In the book: "Abstracts of Papers of the 5th All-Union Symposium on Laser Emission Propagation in the Atmosphere", Tomsk, p. 49-53 (in Russian).

ORTON, G. S., 1975. The thermal structure of Jupiter. I. Implications of Pioneer 10 infrarred radiometer data. *Icarus, vol. 26,* No. 2, p. 125-141.

ORTON, G. S., 1975. The thermal structure of Jupiter. II. Observations and analysis of 8-14 micron radiation. *Icarus, vol. 26,* No. 2, p. 142-158.

TOON, O. B., J. B. POLLACK, C. SAGAN, 1977. Physical properties of the particles composing the Martian dust storm of 1971-1972. *Icarus, vol. 30.* No. 4, p. 663-696.